Naval Research Laboratory

Washington, DC 20375-5320

NRL/MR/7322--19-9871

Development of a Forecast Model for the Lower Pearl River Basin

Cheryl Ann Blain

Ocean Dynamics and Prediction Branch
Oceanography Division

Mustafa Kemal Cambazoglu

Division of Marine Science
University of Southern Mississippi

April 12, 2019

REPORT DOCUMENTATION PAGE

Form Approved
OMB No. 0704-0188

1. REPORT DATE *(DD-MM-YYYY)*	**2. REPORT TYPE**	**3. DATES COVERED** *(From - To)*
12-04-2019	Memorandum Report	01 Nov 2013 - 31 Dec 2016

4. TITLE AND SUBTITLE

Development of a Forecast Model for the Lower Pearl River Basin

5a. CONTRACT NUMBER

5b. GRANT NUMBER

5c. PROGRAM ELEMENT NUMBER

6. AUTHOR(S)

Cheryl Ann Blain and Mustafa Kemal Cambazoglu*

5d. PROJECT NUMBER
Division Serial #73164

5e. TASK NUMBER

5f. WORK UNIT NUMBER
1B37

7. PERFORMING ORGANIZATION NAME(S) AND ADDRESS(ES)

Naval Research Laboratory
1005 Balch Blvd
Stennis Space Center, MS 39529-5001

8. PERFORMING ORGANIZATION REPORT NUMBER

NRL/MR/7322--19-9871

9. SPONSORING / MONITORING AGENCY NAME(S) AND ADDRESS(ES)

St. Tammany Parish Government
21490 Koop Drive
Mandeville, LA 70471-7506

10. SPONSOR / MONITOR'S ACRONYM(S)

St. Tammany Parish Gov., LA

11. SPONSOR / MONITOR'S REPORT NUMBER(S)

12. DISTRIBUTION / AVAILABILITY STATEMENT

DISTRIBUTION STATEMENT A: Approved for public release; distribution is unlimited.

13. SUPPLEMENTARY NOTES

*The University of Mississippi, 118 College Drive, Hattiesburg, MS 39406-0001

14. ABSTRACT

A numerical model for the Lower Pearl River Basin, a braided river system and its floodplain, is developed for the finite element-based coastal model, ADCIRC. Validation of water level prediction is confirmed for Hurricane Isaac in August, 2012 at five hydrographs (Pearl River at Walkiah Bluff near Industrial, MS (WSWM6); Pearl River above Slidell, LA (PRBL1); Pearl River above Slidell, LA (WPSL1) on the West Pearl River; NSTL Station near Stennis, MS (NAPM6); and Pearl River near CSX Railroad near Claiborne (EPCM6) on the East Pearl River)). Results indicate 1) minimal water level error occurs at the river mouth, 2) peak water levels are generally well represented and are within 0.5 m of measured flood stage, and 3) prior to the storm, larger errors in simulated water levels along the West Pearl channel likely indicate mismatches between the model and local in situ depth variations. Other useful analyses include a capacity analysis of the braided river channels based on low, average, and high flow conditions from 2014, and a sensitivity analysis of water level and currents to bathymetry, bottom friction coefficient, and land slope representation.

15. SUBJECT TERMS

Pearl River	MS	Braided Rivers	Total Water Level
Storm Surge	Hydrographs	Forecast Model	Flooding

16. SECURITY CLASSIFICATION OF:			**17. LIMITATION OF ABSTRACT**	**18. NUMBER OF PAGES**	**19a. NAME OF RESPONSIBLE PERSON**
a. REPORT	**b. ABSTRACT**	**c. THIS PAGE**			Cheryl Ann Blain
Unclassified Unlimited	Unclassified Unlimited	Unclassified Unlimited	Unclassified Unlimited	42	**19b. TELEPHONE NUMBER** *(include area code)* (228) 688-5450

Standard Form 298 (Rev. 8-98)
Prescribed by ANSI Std. Z39.18

This page intentionally left blank.

Table of Contents

This page intentionally left blank.

EXECUTIVE SUMMARY

The aim of this study is to construct a modeling system that will inform flood risk management strategies for the Lower Pearl River Basin in coastal Louisiana and Mississippi. The model configuration consists of a hydrodynamic model (ADCIRC) of the Lower Pearl River Basin (LPRB) that receives tidal forcing and water levels at its open water boundary in addition to river discharge hydrographs as forcing at two upstream flux locations near Bogalusa, LA (BXAL1) and Bogue Chitto, LA (BSHL1). A constructed unstructured mesh of triangles resolves the East and West Pearl River channels as well as the interconnected braided channels located between these two main river arteries. High resolution on the order of 4m in channels and 250m offshore extends from the coastline to approximately 75km inland to upstream reaches of the river. The modeling system produces water levels and depth-integrated currents throughout the LPRB and allows for overbank flow into the adjacent floodplain. A sensitivity analysis using a model that contained only the LPRB braided river channel system considered recorded low-flow, average-flow, and high-flow scenarios from 2014 at BXAL1. Stability of the model predictions were found to be slightly sensitive to slope of the river channels and bed stress. More importantly, model results were shown to be highly sensitive to the channel depth or bathymetry. These depths control the discharge capacity of the typically narrow river channels. Under high flow conditions, abnormally elevated currents and water levels were produced in the channel only model, suggesting that in reality overbanks flows occur under such conditions or localized shoreline and depth variations due to log jams, heavy siltation or other causes are not captured in the model representation. The discharge capacity analysis motivated the need to include the surrounding floodplain into the channel model. More realistic bathymetry and topography of the LPRB and its floodplain permits flooding scenarios to be simulated using the wetting and drying capability of ADCIRC. Sensitivities of the LPRB model to various forcing and parameter selections were conducted to assure a robust modeling system. Application of the developed LPRB floodplain model to the 2012 Hurricane Isaac that impacted the region serves as a benchmark for evaluating performance of the forecast water levels. Hurricane Isaac included incoming surge up the Pearl River as well substantial rainfall that resulted in a large quantity of freshwater flow downstream. Comparisons between forecast and measured water level hydrographs at five stations distributed along the East and West Pearl Rivers led to the following conclusions: 1) water level predictions at the river mouth are excellent, 2) peak water levels are generally well represented and are within 0.5 m of measured flood stage, and 3) prior to the storm, discrepancies in simulated water levels along the West Pearl channel likely indicate mismatches between the model representation of local depth variations due to the presence of log jams, siltation, or other local effects. Quantitative error measures of water level (correlation coefficient and root mean square error) indicate reasonable performance of the model during pre-storm, peak-storm, and post-storm conditions at all stations. The exception is at PRBL1 during the post-storm period. The lack of post-storm winds and the less reliable drainage capability of the model likely contribute to this error. The developed LPRB model with a realistic representation of the Pearl River and its floodplain provides an important tool for decision makers to assess both future flood risk and mitigation efforts.

This page intentionally left blank.

1.0 INTRODUCTION AND BACKGROUND

In 2016, there were fifteen weather and climate disaster events with losses exceeding $1 billion each across the United States. Four of these were flooding events, three of which took place in the southeastern United States (NOAA, 2017). Coastal flooding has become one of the major recurring disasters in the Southeastern states of Louisiana and Mississippi in the United States. The coastlines, coastal habitats and coastal urban areas are not only vulnerable to major storm events such as hurricanes which bring multiple disaster agents such as winds and waves but also under major risk of inland river flooding due to heavy precipitation. Coastal ocean model forecasts can be one of the tools in decision making efforts before and during such disaster events. For this reason, accurately resolving rivers in coastal ocean model systems should be very important to support flood risk assessment efforts.

The Pearl River basin drains approximately 8,760 sq. mi. (23,000 sq. km.) in the southeastern United States and is one of the major river systems that flows into the Mississippi Sound in the northern Gulf of Mexico (Patrick, 1995). Nearly 9 percent (760 sq. mi.) of drainage consists of the Lower Pearl River basin (Figure 1) and the connection of the Lower Pearl River Basin to the coastline makes it susceptible to flooding from storm surge during hurricane and tropical storm events in addition to flooding caused by heavy rainfall in the basin.

Approximately 12,700 structures are located in the Lower Pearl River Basin in the state of Louisiana which makes it a crucial area for emergency managers to warn the residents of potential flood events. Local authorities also desire to quantify the impact of proposed storm surge mitigation scenarios on the river and its surrounding flood plain. Coastal flooding may result either from coastal storms that make landfall in the area bringing significant storm surge as well as heavy precipitation with them, or from inland storm events farther upstream that lead to increased river discharge and stages as the rainfall-runoff from multiple watersheds collectively flows into the river channels.

The Lower Mississippi River Forecast Center (LMRFC) is one of the 13 NOAA National Weather Service (NWS) centers in the United States that makes decisions on flood risk management control strategies and is responsible for warning local authorities and emergency managers before and during flood events. LMRFC covers the watersheds that flow into the Gulf of Mexico on the Louisiana and Mississippi coastlines, including the Pearl River basin (Figure 1). In recent years, NOAA-NWS has found that past empirical relationships relating discharge to river stage and flood potential within the Lower Pearl River Basin are unreliable in forecasting flood risk in coastal areas of the Pearl River basin below Pearl River at the Pearl River station on the West Pearl River, as shown in Figure 1. Federal and local government partners joined with research partners to address such needs and interests in regards to flood risk management and mitigation with an objective to develop a modeling system that simulates existing conditions in the Lower Pearl River Basin for water levels and currents. This model can serve as a tool for analyses of past major events and also for predicting future events that will enable improved warning and management strategies.

Manuscript approved April 5, 2019.

There have been two significant flooding events in the Lower Pearl River basin in recent years. In August 2012, Hurricane Isaac made landfall in Louisiana near Port Fourchon, LA approximately 100km south-southeast of the West Pearl River mouth. Isaac was a category 1 hurricane during initial landfall and continued to make multiple landfalls while slowly moving inland towards the north. Widespread flooding developed with Hurricane Isaac over southwestern Mississippi and southeastern Louisiana. More than 20 inches of rain caused the rivers to rise more than 10 ft. above their flood stages and caused moderate to record flooding. Significant flooding developed in many parishes of Louisiana and counties of Mississippi with new flood records set at multiple rivers. Minor to major flooding was also observed at the main channels and tributaries of the Pearl River (NWS, 2012). The heavy rainfall combined with more than 13 feet of storm surge recorded in Lake Borgne caused by Hurricane Isaac resulted in a total of 34 deaths in 3 different counties on its way from Atlantic Ocean to the continental US, and the total damage to the US was estimated to be approximately 2.35 billion (NHC, 2013). Figure 2(a) shows the precipitation map during Hurricane Isaac.

In March 2016, the deep tropical moisture was funneled into parts of the Gulf Coast States and the Mississippi River Valley causing heavy rainfall in southeastern United States and historic flooding across the region (Breaker et al. 2016). 27 inches of precipitation occurred within a short amount of time and river crests reached record highs. Damages from the flood across 5 states were estimated at 1.3 billion USD and the event caused more than 10 million USD disaster cost only in Louisiana. Figure 2(b) shows the 3-day precipitation map and the very heavy precipitation over the states of Mississippi, Louisiana, Texas, and Tennessee. Figure 3 shows the predicted flood inundation around the Pearl River based on high water marks collected by USGS hydrographers (Breaker et al., 2016). It may be seen that the March 2016 heavy rainfall event caused significant flooding in the communities of St. Tammany Parish and the city of Slidell in Louisiana. More than 935 structures were reported damaged in 40 counties across Mississippi.

Recent modeling efforts put more emphasis in modeling rivers in coastal areas in order to be able to capture the combined effects of inland propagating coastal storm surge and flooding due to high river stages upstream. Ding et al. (2012) used an integrated coastal process model to model storm flooding and showed that channel geometry and discharge boundary condition are very important for adequately predicting local flooding conditions. A new computational mesh was developed based on the SL15 ADCIRC grid which has been used for storm surge applications in Gulf of Mexico and East coast US (Bunya et al. 2010). A coupled modeling system that connects a hydrological model to a hydrodynamic model producing total water level simulations for flooding in coastal watersheds was developed for the Tar-Pamlico and Neuse River basins of North Carolina under the CI-FLOW project (Van Cooten et al. 2011). An initial approach to couple these model components would be to insert a hydraulic river model between the hydrologic and hydrodynamic model components to handle fluxes in the coastal floodplain. A second approach would be to extend the hydrodynamic model upstream applying a simplified river channel geometry to allow surge to propagate inland. Dresback et al. (2013) employed the second approach for both the

Tar and Neuse rivers and forecast river discharges were passed to the hydrodynamic model, ADCIRC, at upstream river flux boundary hand-off locations.

McKay and Blain (2010) extend the approach of Dresback et al. (2013) by developing an unstructured Advanced Circulation Model (ADCIRC) mesh for the East Pearl River, MS that resolves to meter scales the geometry and depths of the channel. For the model of McKay and Blain, model-data comparisons for water level along the East Pearl River were conducted at a USGS station at the CSX railroad bridge near Claiborne, MS (USGS301141089320300) and at two additional mooring stations located on East Pearl River. Simulated currents when compared to observed currents measured by a Naval Research Laboratory deployed side-looking Acoustic Doppler current meter (ADCP) station demonstrated the model's capability in precisely capturing the phase and timing of the tidal water level and current variation as well as strong skill in capturing the neap-spring tide magnitude. While this model was a first attempt to model dynamics in the Lower Pearl River Basin, it largely included only the East Pearl River channel, ignoring contributions from the West Pearl River, LA. Furthermore, McKay and Blain (2010) applied a synthetic bathymetry profile along the East Pearl River that was not specifically validated by observed depths. The simulation period spanned a 2-week time period in May 2009 under low flow (500 cfs) conditions. River flux was prescribed at the upstream boundary (Bogalusa, LA) and tidal forcing was applied in constituent form at the open ocean boundary. This model laid the groundwork for a more realistic modeling system that resolves all channels within the Lower Pearl River Basin including its braided channel network within the floodplain of the East and West Pearl River main channels. Development of such a model is the focus of this work.

The aim of this research effort is to develop a high-resolution numerical coastal forecast modeling system that can reasonably predict water levels and current velocities in the Lower Pearl River Basin. Included in such a capability is the capture of overbank flows that result in flooding of the floodplain or inundation of the floodplain due to inland propagating surge. Upon development, Hurricane Isaac will provide a realistic benchmark with which to evaluate the developed LPRB model.

2.0 PEARL RIVER BASIN STUDY AREA

The Pearl River is approximately 44 mi. long, originates in Edinburgh, MS and flows south before it splits into two distinct channels south of Bogalusa, LA to form the East and West branches of the Pearl River. Water from both Pearl River branches flow into Lake Borgne, continue into the Mississippi Sound and eventually flow into the Gulf of Mexico (Figure 1). The West Pearl River flows into Lake Borgne and the Rigolets in Louisiana while the East Pearl River forms the political boundary between the states of Louisiana and Mississippi and flows directly into the Mississippi Sound. Both channels have a strong tidal influence especially during low discharge conditions and regularly flood and drain the intertidal marshes near the river mouth (McKay and Blain, 2010).

The study area covers the Lower Pearl River Basin in southern Mississippi and southeastern Louisiana. Coastal waters in the Mississippi Sound where the Pearl River discharges are covered in the study area to allow for storm surge propagation upriver. The LPRB reaches approximately 75km inland from the coastline with Bogalusa, LA as the northern-most point of the study area.

Historically, the West Pearl River had higher flows because it was the larger branch at the northern split (NASA, 1992). However, the East Pearl River is much wider in its lowest reaches and recent imagery, in-situ depth measurements, and other evidence suggest that flow on the West Pearl is diminishing below Interstate-10 (I-10) (Moorhead, 2014).

3.0 NUMERICAL SIMULATOR DESCRIPTION

In this study, the Advanced Circulation Model (ADCIRC) is used as the hydrodynamic modeling system. ADCIRC utilizes the finite-element method to solve a form of the depth-integrated shallow water wave equations (Luettich et al. 1992, Luettich and Westerink, 2004). ADCIRC has been extensively used for storm surge predictions in coastal areas, estuarine and coastal circulation and also recently for riverine modeling (Blain et al. 2012; McKay and Blain, 2010; Blain et al. 2009). The unstructured mesh of ADCIRC provides the high resolution needed to be able to resolve the complex and meandering narrow channels of the Lower Pearl River Basin as well as complexities of the coastline in coastal Louisiana and Mississippi. The model computes water levels, i.e. elevation, and depth-integrated currents, i.e. river flow velocity. Tidal forcing is comprised of harmonic constituents extracted from the FES99 tidal database (Lefevre et al., 2002) along an open water boundary in Lake Borgne at the western end of the Mississippi Sound. River flux is applied as the upstream forcing. The quadratic bottom friction formulation selected to represent bed stress uses a spatially uniform coefficient, C_F=0.003. The wetting and drying capability of ADCIRC is activated to allow overbank flow into the LPRB floodplain.

4.0 SENSITIVITY ANALYSES USING A CHANNEL MODEL OF THE PEARL RIVER

4.1 Channel Model Development

The unstructured mesh of ADCIRC is constructed using a pre-generated file containing river shoreline locations and a file of water depths (bathymetry) at a sampling of river channel cross-sections. Due to lack of accurate field surveys that define all channel banks for the wide study area, aerial remote sensing imagery was used to identify the river channels in areas where no information is available (McKay and Blain, 2014). Shoreline extraction from remote sensing imagery has been used in other applications (Gilvear et al. 2004). Louisiana 1m resolution aerial IR Digital Orthoimagery quarter quadrangle (DOQQ) tiles from the LSU LIDAR imagery Atlas were used as the data

source to extract river edge and water point locations (National Mapping Program, 1996). This data was processed to obtain river shoreline coordinates (Blain et al., 2013). Initially, water and land pixels in the imagery are separated based on a hue selection criterion (Tanaka, 2006). This procedure was followed by the detection of water edges using a Laplace edge finding filter technique (Russ, 2002). The resulting river channel network was also cross-checked against recently obtained imagery by unmanned aerial systems (UAS) (Moorhead, 2014). Figure 4 shows detailed sections of the West, Mid, Middle and East Pearl River channels compared to the UAS imagery collected by Moorhead in December, 2014. Excellent agreement between imagery and model channels is evident.

In the early phases of the study, bathymetry measurements were only available for the East Pearl River channel. Comparisons of water depth measurements on the East Pearl River to depth profiles generated via a synthetic cubic relationship between channel width and depth are shown in Figure 5. The comparisons indicate that the synthetic bathymetry profile is adequate to represent water depths along the East Pearl River. This synthetic bathymetry approach was extended to the West Pearl River and all other braided river channels in the system and is expressed as a cubic relationship (Equation 1):

$$d = |x|^{1/3} \qquad (1)$$

in which *d* is the depth of any given interior computational node and x is the distance to the closest river bank. This method tends to result in deeper channels in wider sections of the river and shallower channels in narrower river sections.

The river channel mesh has 139,000 nodes and 219,000 elements with resolution as high as 4m in the narrowest channels of the basin and as low as 250m in open waters near the open water boundary. Figure 6 shows the river channel mesh in perspective to four nearby NWS discharge stations at Bogalusa (BXAL1), Bogue Chitto (BSHL1), East Hobolochitto (MNLM6) and West Hobolochitto (CREM6). Depicted in the inset are the West, Mid-, Middle- and East Pearl river channels represented with high resolution in the constructed mesh. For the river channel mesh in Figure 6, applied discharge at the northern most boundary will be derived from conditions at Bogalusa, LA.

4.2 Sensitivity Analyses

To better understand the response of the LPRB river network to upstream discharge, the channel model was executed for 14 day simulation periods, with the first 4 days used to gradually ramp up the external tidal and riverine forcing. Initial simulation sets applied constant streamflow at the upstream flux boundary for representative high, average, and low flow conditions for the Pearl River (40,000, 10,000 and 3,000 cfs). These upstream flux conditions were derived considering the annual average flow rate at Bogalusa (BXAL1) during 2014 (10254 cfs). This annual average was exceeded only once during an April, 2014 event for which fluxes near 40,000 cfs were measured; the the high flow rate of 40,000 cfs. The low flow rate of 3000 cfs derived from the lowest

rate during the six month period from 1 July -31 December 2014 (2997 cfs). At low flow conditions, simulated water levels and currents appear reasonable while water levels and currents predicted in river channels start to rise to uncharacteristically high values for the average flow case. Extremely high water levels and unrealistically high currents are predicted for high flow conditions for the Pearl River channel model.

A sensitivity analyses was conducted to understand the sources of error in high discharge scenarios. The sensitivity analyses included considerations of the friction coefficient, water depth and channel slope. The sensitivity to friction coefficient was evident, especially for currents, but all modeled results were realistic within a C_f range from 0.0001 to 0.020 as shown in Figure 7 for downstream sections of the West and Middle Pearl. Results in the East Pearl are not shown because differences in velocities and water levels for varying friction coefficients are quite small. From Figure 7, water levels in lower reaches of the river channels were essentially insensitive to different friction coefficients within the range examined while currents were clearly affected by the level of bed stress. Velocities for friction coefficients higher than 0.010 were much smaller than those with friction coefficient values lower than 0.003. Considering the friction coefficients used for earlier studies in the region, further model simulations are conducted using a friction coefficient value of 0.001.

After applying the synthetic river channel depths based on Equation (1), a realistic channel bathymetry is constructed by tilting the mesh from the coastline to upstream locations using a representative constant slope for the entire domain. A constant and representative channel slope of -3.3832E-04 was calculated and used for all the channels within the Pearl River channel model. In reality, certain parts of the river have steeper slopes while other sections have milder slopes based on actual topography. In fact, the slopes at the downstream reaches of the basin were found to be milder than the constant slope used. Figure 8 shows the variation of the channel slopes calculated for different segments of the river from the upstream boundary to the coastline based on the topography values provided in the ADCIRC model SL16 mesh (Dietrich et al., 2011). Upstream segments (segments 1, 2, 3, 10, 11) have the steepest slope while most of the West Pearl (segments 5 thru 9) and the downstream section of the East Pearl (segment 14) have milder slopes. The mid-section of the East Pearl River (segment 12) has a slope identical to that applied initially to the entire system.

To consider the role of channel depth in the computations of water level and currents, Figure 9 shows the computed velocity and elevation variations for the high flow scenario subject to a constant friction coefficient, $C_f = 0.001$, at two different constant channel depths, 10m and 15m. The results are shown for downstream locations on the Pearl River with a location on the West Pearl at 30.3N and on the East Pearl farther downstream at 30.2N. From Figure 9, the mean water level and velocities increase during the first 4 days of the simulation when the forcing is ramped up. After Day 4, the water levels and velocities vacillate around this mean value due to tidal fluctuations for water depths equal 15 m. The mean velocity of 0.35 m/s on the West Pearl is higher than that on the East Pearl with values of 0.1 m/s, while the ranges of velocity and water level are similar in both channels. When water depths are 10m, the velocity and water levels in the West Pearl do not reach a steady state following the ramp period. Rather

they continue to increase even at Day 8 of the simulation time period. For this case, the velocity range on the East Pearl is higher (0.2 m/s) than that of the West Pearl. Computed water levels on East Pearl are not affected by the bathymetry changes at this downstream location. The results indicate that there is a critical depth between 10m and 15m at which channel model stability is disturbed.

Figure 10 demonstrates the effect of channel depth and channel slope on model predictions at 30.45N on both the West Pearl and East Pearl River. Once again velocities and elevations (water levels) within both main branches of the Pearl River reach a steady mean with fluctuations around that mean for a constant water depth of 15m (black lines). In contrast, water level and velocities at the mid-latitude locations on both the West and East Pearl continuously increase for the first 8 days of the simulation when the water depth is set at a constant 10m (green lines). When a milder constant channel slope is applied to the constant 10m depth case, the water levels and velocities stabilize. This is likely because using milder slopes in lower reaches of the basin resulted in a decrease in velocities which did not exceed the capacity of the river channels. These results show the importance of accurate channel bathymetry and topography to achieve realistic predictions of water level and velocity in river channels.

Results of the channel model sensitivity analyses indicate that water levels and currents in the West and East Pearl Rivers are most affected by channel depth and to a lower degree the channel slope. Both depth and slope factors in the river capacity which, in turn, is directly related to the ability of the river to contain upstream discharges within the river banks.

4.3 Capacity Analyses

The capacity of the main river channels in the LPRB is analyzed to better understand the development of instabilities during average and high flow conditions. This analysis has been conducted for both the West Pearl and East Pearl Rivers since increased velocities were observed on both main stems of the Pearl River. The maximum channel discharge capacity *(Q*) has been calculated based on Manning's equation:

$$Q = \frac{A}{n} R^{2/3} S^{1/2} \qquad (2)$$

where *A* is the channel cross-sectional area, *n* is a constant roughness coefficient of 0.22, *R* is the wetted perimeter of the channel, and *S* is a representative constant average slope (-3.3832E-04) measured from the upstream boundary to the coastline. The channel area (*A*) was computed by integrating the bathymetry profile over the channel width for all channel boundary nodes. Figure 11(a) shows the discharge capacity (color) of the West and East Pearl River channels from the upstream boundary towards the coastline, while Figures 11(b) and 11(c) show the variation of West Pearl and East Pearl River discharge capacity versus latitude, respectively. The West Pearl capacity is higher than the average flow discharge of 10,000 cfs (Avg. line in Figure 11) while the East Pearl capacity is lower at the same latitudes for the upstream reaches of the river. On the other hand, the East Pearl is wider and can carry more river water at the downstream reaches, south of 30.3N. Multiple choke points with discharge capacity of the river less than the average flow are observed during average flow conditions in both main river

channels. In fact, the river discharge capacity is less than the high flow conditions in modeled stretches of both the West Pearl and East Pearl rivers. Such choke points are indicative that overbank flows must occur at these locations, sending water from the channels into the floodplain under both high upstream discharge and at times simply average upstream discharge conditions. The presence of these choke points in the model could also point to specific locations where the local depths and river geometry may differ from that represented in the model. The presence of log jams, heavy siltation, or other obstructions could cause such choke points; conversely the presence of such localized variation may not be accounted for in the model.

5.0 DEVELOPMENT OF THE FLOODPLAIN MODEL FOR THE LOWER PEARL RIVER BASIN

5.1 Floodplain Model Development

The simulations and analyses derived from the Pearl River channel model have shown a need to expand the modeling capability to include the floodplain of the Lower Pearl River Basin. During high discharge, inclusion of the floodplain will allow overbank flows and flooding and ultimately result in more accurate predictions, not only for inundation, but also the water levels and currents predicted within the river channels themselves. Expansion of the high resolution Pearl River channel model to include the surrounding floodplain is accomplished by incorporating the highly resolved channel mesh into the large domain ADCIRC mesh of US East Coast and Gulf of Mexico (SL16 mesh) used in prior studies for hurricane modeling (Dietrich et al., 2011).

A multistep, manual mesh development process was followed to accomplish this task using the meshing tool, MeshGUI (Blain et al., 2008). Initially, the area covered by the river channel model was cut from the large domain model as shown in Figure 12(a). Then, the channel model was inserted into the voided area as shown in Figure 12(b). The resolution at the channel banks are higher than the surrounding floodplain resolution, therefore a gap was left between the channel mesh and the surrounding floodplain. This gap between the channel mesh river banks and the boundary of the larger domain mesh surrounding the channels was carefully “stitched” together by adding elements with a gradation of size to allow for a smooth transition between elements moving from the channel to the floodplain. A segmented approach was followed due to the meandering nature of the river channels. The voided gaps were carefully meshed segment by segment from the upstream boundary of the mesh to coastline downstream (Figure 12(c)). The final product is a single continuous floodplain mesh for the Lower Pearl River Basin that contains the highly resolved, braided Pearl River channels as shown in Figure 12(d).

The final floodplain model configuration has 421,667 nodes and 842,602 elements maintaining the O(1m) high resolution while providing the floodplain for model wetting and drying to simulate overbank flows and flooding (Figure 13). The final mesh extends south to a boundary in Lake Borgne to the eastern end of Mississippi Sound in

the northern Gulf of Mexico where tidal forcing from a validated tidal database (Lefevre et al., 2002) is applied. Figure 13(b) and 13(c) compare the mesh resolution of the larger domain US East Coast model (SL16) around the West Pearl river channels with the resolution of the floodplain model developed for this study. Model bathymetry and slope are realistically captured as shown in Figure 14, based on the topographic values of the SL16 mesh used for Hurricane Gustav (2008) simulations in the area (Dietrich et al., 2011). Upstream discharge is to be applied at specified flux boundaries necessarily located at the edge of the domain shown in Figure 14.

The location of the flux boundary for the main stem of the Pearl River, just north of the East-West split, is identified in Figure 15 as Bogalusa, LA. Discharges from the gauge USGS 02489500 Pearl River near Bogalusa, LA (BXAL1) are applied at this location. The signature of a second tributary, Bogue Chitto, is barely evident in Figure 15 and its confluence with the West Pearl River is located inside the domain boundaries. Since the Bogue Chitto contributes significantly to the upstream flow in the Pearl River Basin, an extension to the West Pearl River channel is constructed to represent the Bogue Chitto. The imagery analysis techniques of Blain et al. (2013) and McKay and Blain (2014) are applied to the Bogue Chitto as shown in Figure 16. The derived mesh shown in Figure 16 is inserted into the LPRB floodplain model using the techniques outline in Figure 12. A flux boundary can now accommodate discharge contributions from the Bogue Chitto gauge, USGS 02492000 Bogue Chitto River near Bush, LA (BSHL1). Water depths along the Bogue Chitto channel are obtained using the cubic, synthetic bathymetry relationship described earlier. The Bogalusa and Bogue Chitto discharge locations in the LPRB model serve as hand-off locations for NOAA/NWS gage hydrographs associated with stations of the same name.

5.2 Sensitivity Tests of the Floodplain Model

Water levels from the new floodplain model for an average flow scenario are shown in Figure 17. For this realization, only discharge from the Bogalusa, LA station was active. Tidal-induced water level changes may be seen traveling into Lake Pontchartrain via the Rigolets in Figure 17 for two times approximately 8 hrs and 40 min apart. The tides will also travel upstream into all of the Pearl River braided channels. This result indicates river flow coming downstream while remaining within the river channels due to flux initiated at the upstream boundary. No flooding from the upstream river flux is observed as expected under low flow conditions. An area along the northeastern shore of Lake Pontchartrain that was initially dry, wetted during this simulation demonstrating the functionality of the wetting/drying mechanism within the modeling system.

Further realizations of the low, average and high flow scenarios are found in Figures 18 and 19. All told approximately 25 different simulations (not all reported here) were executed in which model parameters associated with the boundary flux type, wetting/drying configuration, tidal forcing, model equation formulation (lumped matrix solution), friction value, surface roughness specification, and boundary flux values were varied to assure the robustness of the Pearl River floodplain model.

6.0 VALIDATION OF THE FLOODPLAIN MODEL FOR HURRICANE ISAAC (2012)

6.1 Model Configuration

The test case selected to evaluate the Lower Pearl River Basin (LPRB) floodplain model comes from Hurricane Isaac (August, 2012) conditions which brought both extreme rainfall and surge to the Lower Pearl River Basin. Simulations of the LPRB model for Hurricane Isaac extend for 14 days from 23 August 2012 through 03 September 2012. The landfall of Hurricane Isaac occurred on 29 August at 1900 west of New Orleans, LA and the LPRB. Hurricane Isaac brought torrential rains to the watersheds feeding the LPRB. To capture these freshwater effects, upstream discharge hydrographs at Bogalusa, LA (USGS 02489500 Pearl River near Bogalusa, LA – BXAL1) and the Bogue Chitto (USGS 02492000 Bogue Chitto River near Bush, LA – BSHL1) are used to force the model. At the same time offshore water levels were elevated by the simultaneous occurrence of surge and tides. Realistic water levels generated by Hurricane Isaac's tide and surge are captured by extracting predicted water levels from a large domain ADCIRC simulation of Hurricane Isaac (Figure 20). The large domain model uses the Louisiana Coastal Protection and Restoration Authority (CPRA) surge and inundation mesh (Figure 20(a)) designed for the simulation of Hurricane Isaac and described in detail by Cobell et al. (2013). NOAA's best available reanalysis h*Wind product for Hurricane Isaac was processed and applied as surface forcing to the CPRA mesh to reproduce tide and surge conditions during Hurricane Isaac. A 16-day ramp-up period is designed to spin up tides during the initial 14 days and winds the remaining 2 days. The last h*Wind product available is at 29 August 2012 1930 after which winds diminish to zero in the simulation.

The open water boundary points (blue) of the LPRB model are overlain on the large domain simulation of surge for Hurricane Isaac in Figure 21. An example of the hydrograph that is extracted from the large domain solution is also shown. These water level hydrographs at every open water boundary point provide the offshore tide and surge forcing that propagates up into the river channels and the LPRB.

6.2 Model-Data Comparisons

Five National Weather Service (NWS) hydrographic stations recorded water levels during Hurricane Isaac and are identified in Figure 22. These stations are Pearl River at Walkiah Bluff near Industrial, MS (WSWM6), Pearl River above Slidell, LA (PRBL1), and Pearl River above Slidell, LA (WPSL1) on the West Pearl River, and NSTL Station near Stennis, MS (NAPM6) and Pearl River near CSX Railroad near Claiborne (EPCM6) on the East Pearl River. These station observations are used to evaluate the performance of the LPRB model at three temporal stages of the Hurricane Isaac event, pre-storm (23 August 2012 2100 to 29 August 2012 0900), peak-storm (0900 29 August 2012 to 31 August 2012 0000), and post-storm (31 August 2012 0000 to 03 September 2012 0000).

Overall model-data comparisons (Figure 23, 24, and 25) indicate that error is minimal at station EPCM6 (CSX Railroad near Claiborne), near the outlet of the East Pearl River to the Mississippi Sound. The timing of peak surge is also well represented at all stations, including WSWM6 (Walkiah Bluff near Industrial MS), whose peak water levels on September 2 are largely a result of rainfall. Non-coincidentally, each of these stations lie along the East Pearl River where river depth values in the model agree well with available measurements. All modeled peak flood stages are within 0.5 m of the measured flood stage. However, prior to the storm, (i.e. Aug. 26), simulated water levels exhibit larger discrepancies along the West Pearl channel. There may be local variations in bathymetry or shoreline not represented in the model that may account for these differences. Larger RMSE at the West Pearl Station (PRBL1) during the post-storm period may reflect the lack of storm winds (zero wind is assigned after 29 August 2012 1930). Furthermore, the mechanisms for draining flooded areas are not well represented in the existing model and this may impact post-storm predictions.

7.0 SUMMARY AND CONCLUSIONS

This study has shown the capability of the Advanced Circulation Model, ADCIRC, for simulating riverine flow in a complex, braided river system, specifically the Pearl River in the Lower Pearl River Basin. A developed channel mesh resolves the main West Pearl and East Pearl river channels as well as the highly complex mid-, middle- Pearl channels at O(m) resolution. A series of sensitivity analyses indicated that model stability is assured for low flow and typically maintained for average river flow conditions. Unrealistically elevated water levels and currents occurred during a high river flow conditions. Channel depth was found to be the most sensitive river parameter when considering depth, bed stress and slope. An examination of river capacity reveals that at high flow, and at times, average flow conditions the capacity of the river to transmit high flow events was exceeded and that such fluxes could result in overbank flow at identified choke points. These choke points may also indicate that the water depths or shoreline in the model do not accurately represent local conditions due to log jams or excess siltation. This exceedance of the river capacity at high flow demonstrates a need for developing a LPRB river model that includes the floodplain surrounding the river channels.

The details of constructing a floodplain model with high resolution in the channels connected seamlessly to the surrounding floodplain are presented. Sensitivity tests of the LPRB floodplain model for average flow conditions demonstrate the functionality of the model to simulate downstream freshwater fluxes while allowing tides and surge to propagate northward into the floodplain and river channels. Many realizations of the low, average and high flow scenarios were executed, modifying boundary types, flux values, and model parameters to assure the robustness of the Pearl River floodplain model.

Finally, the historical Hurricane Isaac that impacted the region in 2012 serves as a benchmark for evaluating performance of the forecast water levels by the developed

LPRB model. Hurricane Isaac included incoming surge up the Pearl River as well substantial rainfall that resulted in a large quantity of freshwater flow downstream. Comparisons between forecast and measured water level hydrographs at five stations distributed along the East and West Pearl Rivers led to the following conclusions: 1) Minimal water level error occurs at the river mouth, 2) peak water levels are generally well represented and are within 0.5 m of measured flood stage, and 3) prior to the storm, larger errors in simulated water levels along the West Pearl channel likely indicate mismatches between the model representation of local depth variations due to the presence of log jams, siltation, or other local effects. Quantitative error measures of water level (correlation coefficient and root mean square error) are computed at each gauge location where measured water levels exist. The simulation period is broken into three segments, pre-storm, peak-storm, and post-storm. Post-storm errors are not unexpected due to the lack of post-storm winds and the less reliable drainage capability of the model. The developed model with a realistic representation of the Pearl River provides an important prediction tool to decision makers for better preparation, protection and mitigation for future flooding events in the study area.

8.0 POTENTIAL LIMITATIONS

While demonstrated to produce reasonable forecasts for water levels under Hurricane Isaac conditions, there are a number of known advances that could be made to the LPRB model to enhance its level of realism. These steps could ultimately improve the quality of the forecasts.

1. Contributions from the East and West Hobolochitto tributaries are not presently accounted for. These winding creeks with dense tree overhang prevents application of the imagery-based tools described within for obtaining accurate shoreline data of the Hobolochitto Rivers. Furthermore, the path of the East and West Hobolochitto Rivers from their entry into the model domain from the east to their intersection with the East Pearl River channel is lengthy, potentially adding lots of spatial resolution and thus computational cost to the model. An alternative is to alter the eastern boundary of the LPRB mesh to allow for insertion of a flux representing the East and West Hobolochitto contribution to upstream discharge in the LPRB system. Model simulations that considered all combinations of flux contributions from the Bogalusa, the Bogue Chitto, and the East and West Hobolochitto tributaries indicated that the latter was of least importance to the overall flow and water levels in the LPRB model.

2. The LPRB model as configured does not include any engineering structures that may exist within the river system. There are inactive weirs, bridge pilings, and potentially other man-made structures that can alter flow patterns. All of these are currently neglected in the developed LPRB model.

3. Water depth measurements made throughout the LPRB and collected by St. Tammany Parish in 2014 and 2015 are shown in Figure 26. The bathymetry values

prescribed in the developed LPRB model are intended to represent the conditions reflected by the measured data. Depths along the East Pearl River channel are exceptionally realistic. The West Pearl River and the braided channels in the flood plain are far more dynamics and as such are continually evolving. Depths for these locations may require local adjustments that reflect the presence of log jams, short term siltation, and other factors that may alter the bathymetry.

9.0 ACKNOWLEDGMENTS

This research was accomplished in part due to a grant from St. Tammany Parish, Louisiana, USA (Agreement NRL-SSC (73)-2013-11. The authors would like to thank Robert Linzell for his contributions during this research and would also like to honor the late Dr. J. Paul McKay for his efforts initiating this research study.

10.0 REFERENCES

Altinakar, M.S., M.Z. McGrath, V.P. Ramalingam, and H. Omari. 201X. 2D modeling of Big Bay Dam failure in Mississippi: Comparison with field data and 1D model results, XYZ Conference, Organizer, pages.

Blain, C.A., R.S. Linzell, A. Weidemann, P. Lyon. 2009. A tool for rapid configuration of a river model. In: Proceedings of Oceans 2009 MTS/IEEE Biloxi Conference, Biloxi, MS.

Blain, C.A., M.K. Cambazoglu, R.S. Linzell, K.M. Dresback, and R.L. Kolar. 2012. The predictability of near-coastal currents using a baroclinic unstructured grid model. *Journal of Ocean Dynamics*. 62(3), 411-437.

Blain, C.A., R.S. Linzell, J.P. McKay. 2013. Simple methodology for deriving continuous shorelines from imagery: Application to rivers. *Journal of Waterway, Port, Coastal and Ocean Engineering*, 139(5), 365-382.

Blain, C. A., R. Linzell, T. C. Massey, and B. D. Estrade. 2008. MESHGUI: A mesh generation and editing toolset for the ADCIRC model, NRL Mem. Rep. NRL/MR/7320-2007-9083, Naval Research Laboratory, Stennis Space Center, MS.

Breaker, B.K., K.M. Watson, P.A. Ensminger, J.B. Storm, C.E. Rose. 2016. Characterization of peak streamflows and flood inundation of selected areas in Louisiana, Texas, Arkansas, and Mississippi from flood of March 2016. U.S. Geological Survey Scientific Investigations Report 2016-5162, 33 p. Available online: https://doi.org/10.3133/sir20165162.

Cobell, Z., H. Zhao, H. J. Roberts, R. R. Clark, and S. Zou, 2013. Surge and wave modeling for the Louisiana 2012 Coastal Master Plan, *Journal of Coastal Research*, SI, 67, 88-108.

Dietrich, J.C., J.J., Westerink, A.B., Kennedy, J.M., Smith, R.E., Jensen, M., Zijlema, L.H., Holthuijsen, C.N., Dawson, R.A., Luettich Jr., M.D., Powell, V.J., Cardone,

Cox, A.T., G.W., Stone, H., Pourtaheri, M.E., Hope, S., Tanaka, L.G., Westerink,

Westerink, H.J. and Z., Cobell. 2011. Hurricane Gustav (2008) Waves and Storm Surge: Hindcast, Validation and Synoptic Analysis in Southern Louisiana. *Monthly Weather Review*, 139(8), 2488–2522.

Dietrich, J. C., C. J. Trahan, M. T. Howard, J. G. Fleming, R. J. Weaver, S. Tanaka, L. Yu, R. A. Luettich, C. N. Dawson, J. J. Westerink, G. Wells, A. Lu, K. Vega, A. Kubach, K. M. Dresback, R. L. Kolar, C. Kaiser, R. R. Twilley, 2012. Surface trajectories of oil transport along the northern coastline of the Gulf of Mexico, Continental Shelf Research 41, 17-47.

Ding, Y., M.S. Altinakar, Y. Jia, S.N. Kuiry, Y. Zhang, and A. Goodman. 2012. Simulation of storm surge in the Mississippi Gulf Coast using an integrated coastal processes model, World Environmental and Water Resources Congress 2012: Crossing Boundaries, ASCE, 1635-1652.

Dresback, K.M., J.G. Fleming, B.O. Blanton, C. Kaiser, J.J. Gourley, E.M. Tromble, R.A. Luettich Jr., R.L. Kolar, Y. Hong, S. Van Cooten, et al. 2013. Skill assessment of a real-time forecast system utilizing a coupled hydrologic and coastal hydrodynamic model during Hurricane Irene (2011). Continental Shelf Research. 71, 78-94.

Gilvear, D., C. Davids, A. Tyler. 2004. The use of remotely sensed data to detect channel hydromorphology; River Tummel, Scotland. River Research and Applications, 20, 795-811.

Lefevre, F., F. Lyard, E. Le Provost, J. Schrama. 2002. FES99: A global tide finite element solution assimilating tide gauge and altimetric information. Journal of Atmospheric and Oceanic Technology.

Luettich, R., J. Westerink, N. Scheffner. 1992. ADCIRC: An advanced threedimensional model for shelves, coasts and estuaries, Report 1: Theory and methodology and ADCIRC-2DDI and ADCIRC-3DL, Tech. Rep. DRP-92-6. Tech. rep., Department of the Army, Washington, DC.

Luettich, R., J. Westerink. 2004. Formulation and numerical implementation of the 2D/3D ADCIRC finite element model version 44.XX.

McKay, J.P., and C.A. Blain. 2010. Toward developing a hydrodynamic flow & inundation model of the Lower Pearl River. Proceedings OCEANS 2009, MTS/IEEE Biloxi – Marine Technology for Our Future: Global and Local Challenges, Biloxi, MS, October 2009.

McKay J.P., C.A. Blain. 2014. An automated approach to extracting river bank locations from aerial imagery using image texture, River Research and Applications, 30(8), 1048-55.

Moorhead, R. 2014. Personal communication. Related online article can be found at: http://www.msstate.edu/newsroom/article/2014/12/mississippi-states-uas-expertisedisplay/

National Weather Service, NWS. 2012. Monthly report for hydrologic conditions, Report for August 2012. Ed: Kenneth Graham, September 15, 2012.

National Hurricane Center, NHC. 2013. Tropical Cyclone Report, Hurricane Isaac (AL092012), 21 August – 1 September 2012. Ed: Ronnie Berg, 28 January 2013.

National Oceanic and Atmospheric Administration, 2017. U.S. billion-dollar weather & climate disasters 1980-2016. Available online at: https://www.ncdc.noaa.gov/billions/.

NASA. 2001. NASA Stennis Space Center, Environmental resource document, inventory summary for John C. Stennis Space Center: Chapter 3. Water Resources, Stennis Space Center, MS, April 2001.

National Mapping Program. 1996. Standards for digital orthophotos. Tech. rep., US Geological Survey.

NASA. 1991. NASA Stennis Space Center, Environmental resource document, inventory summary for John C. Stennis Space Center.

National Mapping Program. 1996. Standards for digital orthophotos. Tech. rep., US Geological Survey.

Patrick, R. 1995. Rivers of the United States: Volume II Chemical and physical characteristics. John Wiley and Sons, Inc.

Roth, M. K., J. MacMahan, A. Reniers, T. M. Ozgokomen, K. Woodall, B. Haus, 2017. Observations of inner shelf cross-shore surface material transport adjacent to a coastal inlet in the northern Gulf of Mexico, Continental Shelf Research 137,142-153.

Russ, J. 2002. Image Processing Handbook, 4th Ed. CRC Press.

SCOPE Experiment surface drifters, Santa Rosa Island, Florida, December 2013. Distributed by: Gulf of Mexico Research Initiative Information and Data Cooperative (GRIIDC), Harte Research Institute, Texas A&M University, Corpus Christi. Available from: https://data.gulfresearchinitiative.org/data/R1.x134.073:0023.

Tanaka, H. 2006. Monitoring of short-term morphology change at a river mouth. In: Proceedings of the Vietnam-Japan Estuary Workshop.

Van Cooten, S., K.E. Kelleher, K. Howard, J. Zhang, J.J. Gourley, J.S. Kain, K. Nemunaitis-Monroe, Z. Flamig, H. Moser, A. Arthur, et al. 2011. The CI-FLOW

project: a system for total water level prediction from the summit to the sea. Bull. Am. Meteorol. Soc. 92 (11), 1427–1442.

Weidemann, P. Lyon. 2009. A tool for rapid configuration of a river model. In: Proceedings of Oceans 2009 MTS/IEEE Biloxi Conference, Biloxi, MS.

11.0 FIGURES

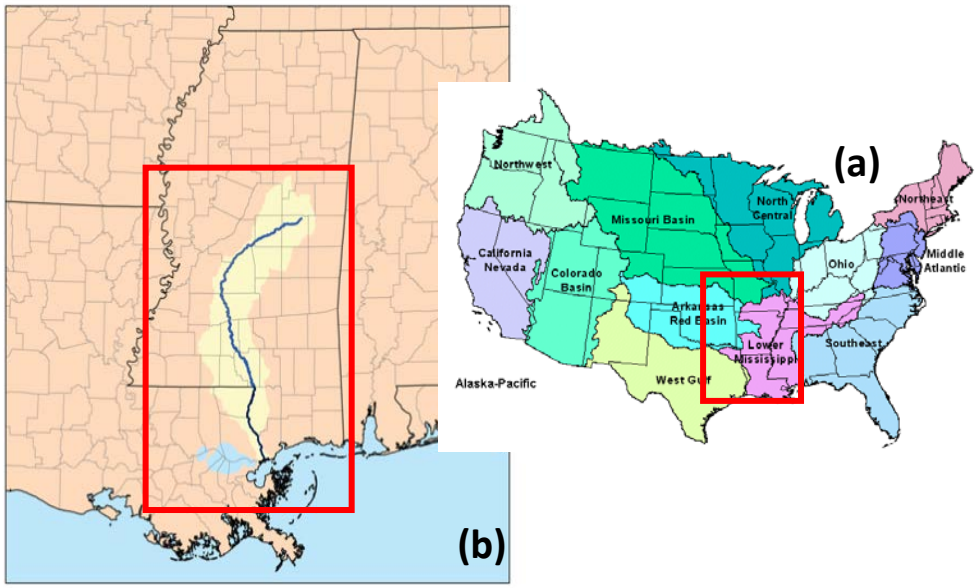
(a)
Northwest
Missouri Basin
North Central
Northeast
California Nevada
Colorado Basin
Ohio
Middle Atlantic
Arkansas Red Basin
Lower Mississippi
Southeast
Alaska-Pacific
West Gulf
(b)

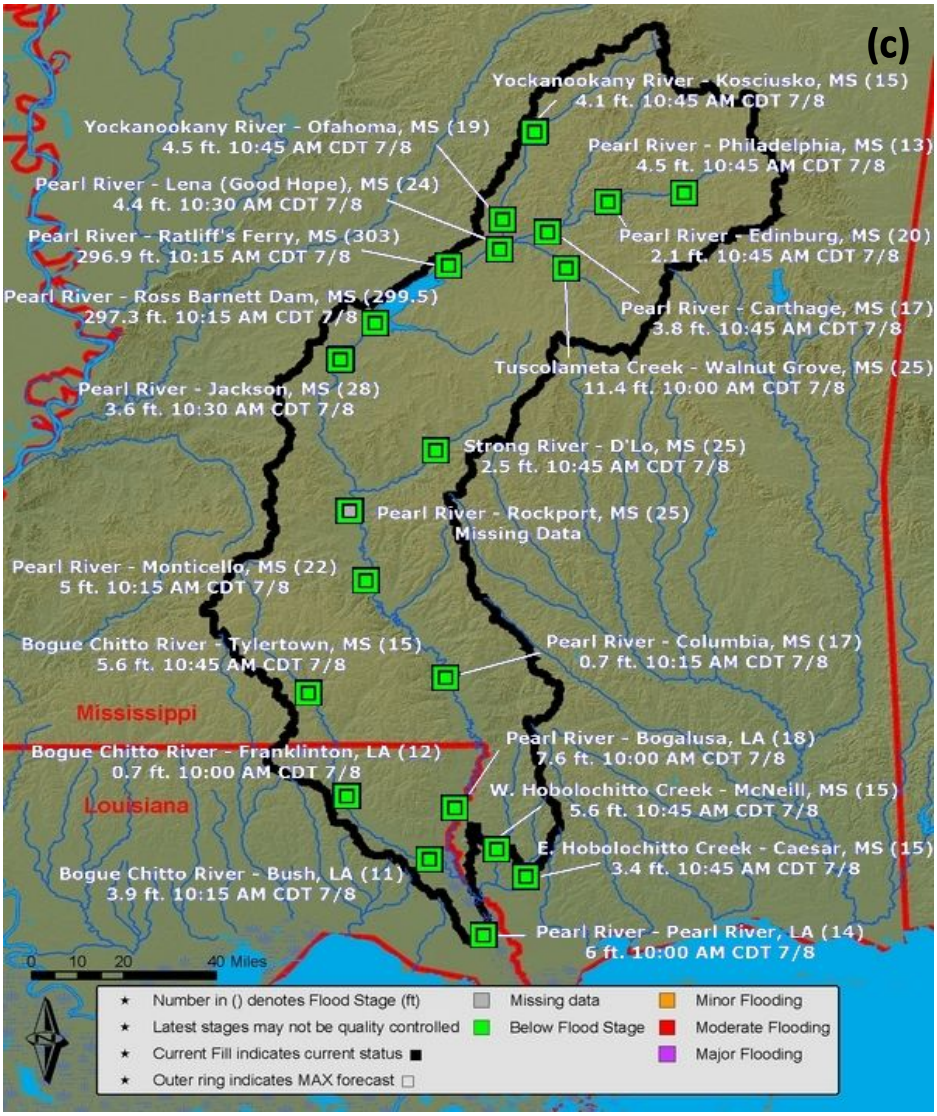
(c)
Yockanookany River - Kosciusko, MS (15)
4.1 ft. 10:45 AM CDT 7/8
Yockanookany River - Ofahoma, MS (19)
4.5 ft. 10:45 AM CDT 7/8
Pearl River - Philadelphia, MS (13)
4.5 ft. 10:45 AM CDT 7/8
Pearl River - Lena (Good Hope), MS (24)
4.4 ft. 10:30 AM CDT 7/8
Pearl River - Ratliff's Ferry, MS (303)
296.9 ft. 10:15 AM CDT 7/8
Pearl River - Edinburg, MS (20)
2.1 ft. 10:45 AM CDT 7/8
Pearl River - Ross Barnett Dam, MS (299.5)
297.3 ft. 10:15 AM CDT 7/8
Pearl River - Carthage, MS (17)
3.8 ft. 10:45 AM CDT 7/8
Tuscolameta Creek - Walnut Grove, MS (25)
11.4 ft. 10:00 AM CDT 7/8
Pearl River - Jackson, MS (28)
3.6 ft. 10:30 AM CDT 7/8
Strong River - D'Lo, MS (25)
2.5 ft. 10:45 AM CDT 7/8
Pearl River - Rockport, MS (25)
Missing Data
Pearl River - Monticello, MS (22)
5 ft. 10:15 AM CDT 7/8
Bogue Chitto River - Tylertown, MS (15)
5.6 ft. 10:45 AM CDT 7/8
Pearl River - Columbia, MS (17)
0.7 ft. 10:15 AM CDT 7/8
Mississippi
Pearl River - Bogalusa, LA (18)
7.6 ft. 10:00 AM CDT 7/8
Bogue Chitto River - Franklinton, LA (12)
0.7 ft. 10:00 AM CDT 7/8
W. Hobolochitto Creek - McNeill, MS (15)
5.6 ft. 10:45 AM CDT 7/8
Louisiana
E. Hobolochitto Creek - Caesar, MS (15)
3.4 ft. 10:45 AM CDT 7/8
Bogue Chitto River - Bush, LA (11)
3.9 ft. 10:15 AM CDT 7/8
Pearl River - Pearl River, LA (14)
6 ft. 10:00 AM CDT 7/8
0 10 20 40 Miles
★ Number in () denotes Flood Stage (ft)
★ Latest stages may not be quality controlled
★ Current Fill indicates current status ■
★ Outer ring indicates MAX forecast □
Missing data
Below Flood Stage
Minor Flooding
Moderate Flooding
Major Flooding

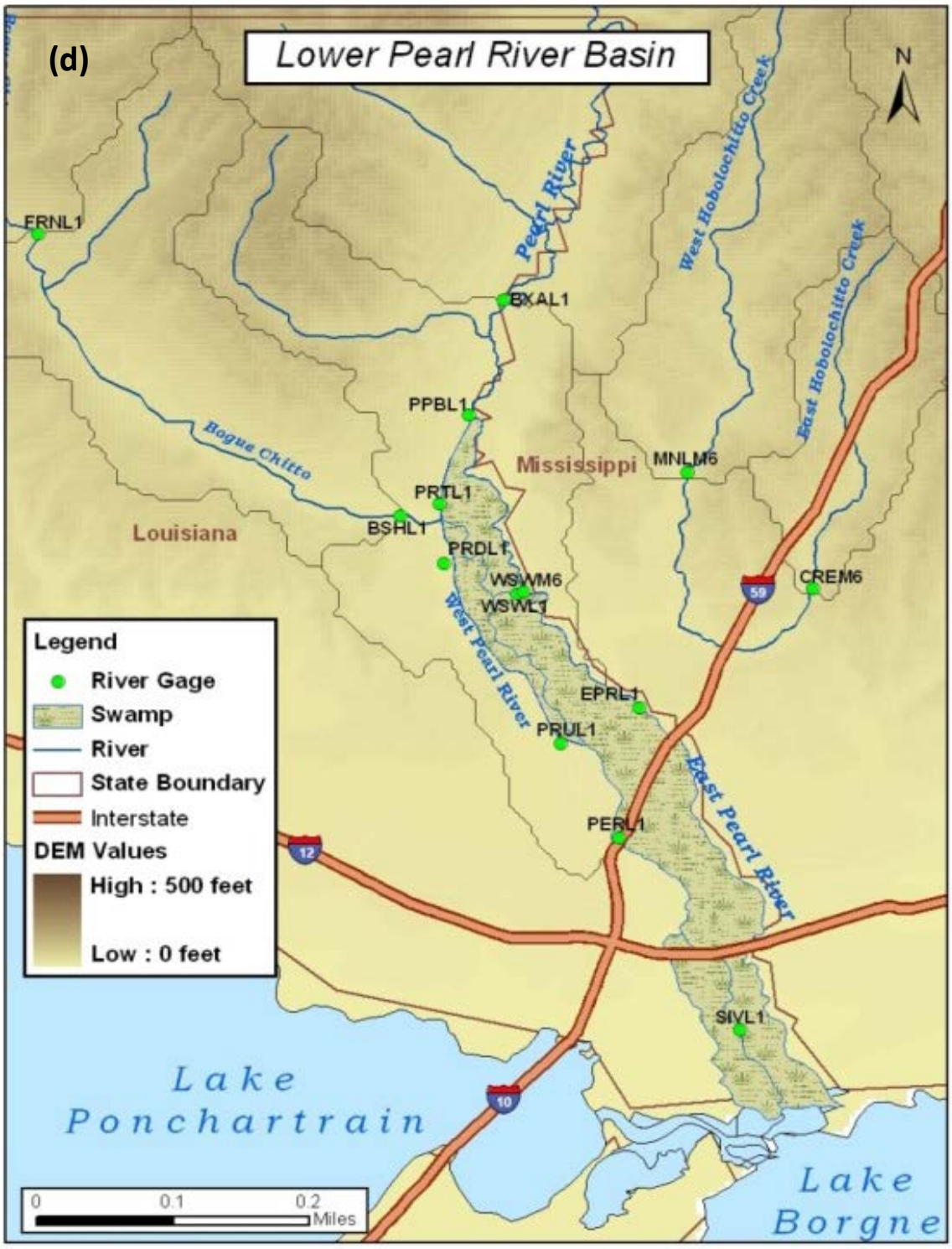

Figure 1 – (a) NOAA National Weather Forecast Center areas, (b) Lower Mississippi River Forecast Center (LMRFC) area, (c) Pearl River basin with LMRFC river gage locations, (d) Lower Pearl River basin with LMRFC river gages showing Pearl River at Pearl River station in black circle (PERL1).

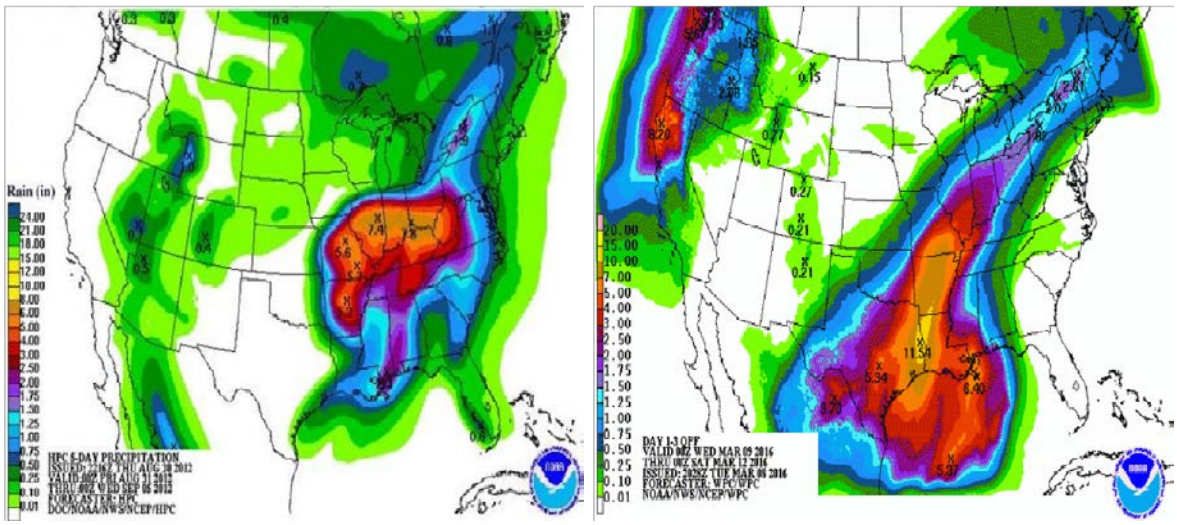

Figure 2 – (left) Precipitation map over continental US from August 31 to September 5, 2012, (right) Precipitation map over continental US from March 9 to March 12, 2016.

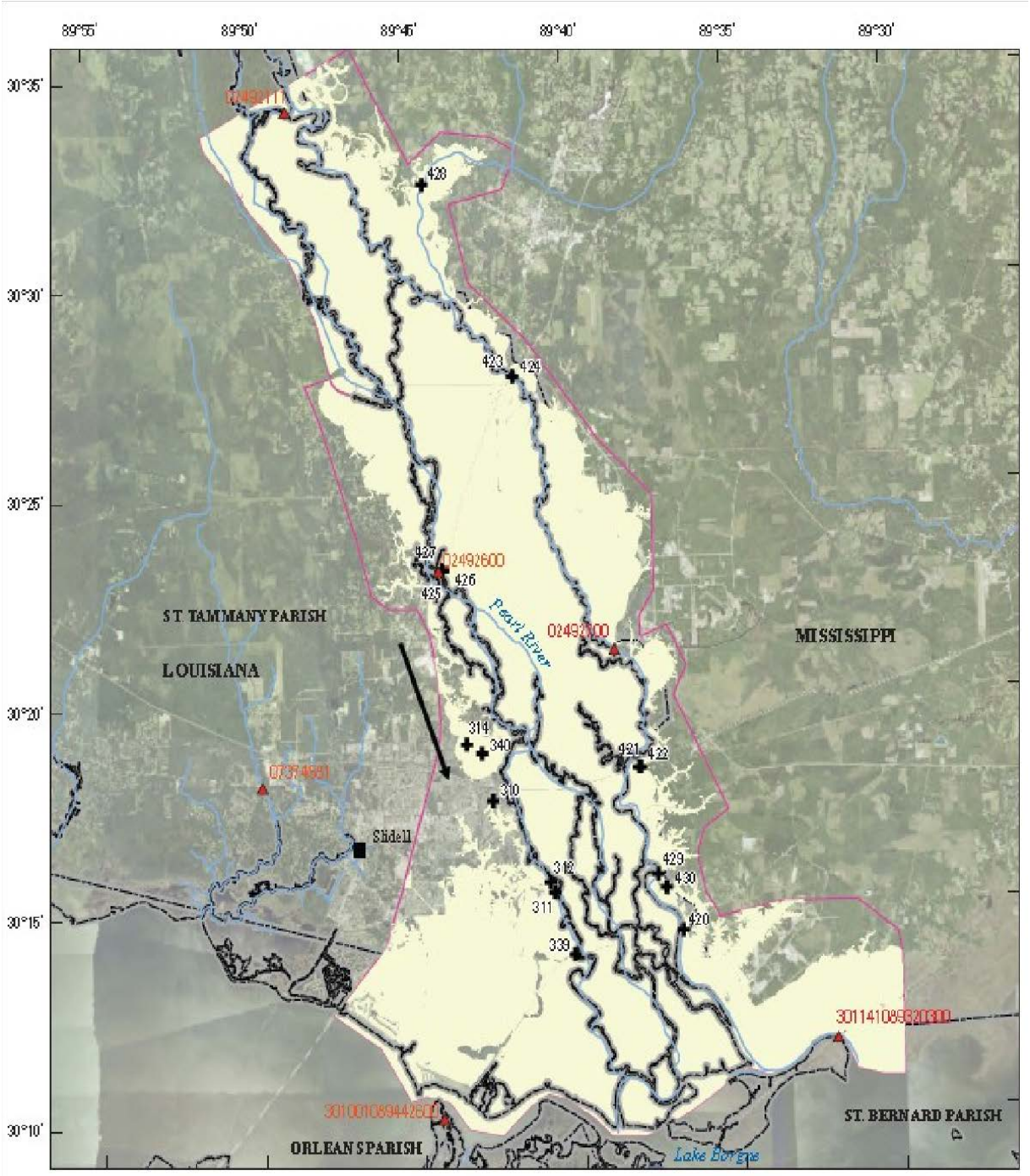

Figure 3 – Flood inundation map around Pearl River in March 2016 based on USGS high water marks (adapted from Breaker et al. 2016).

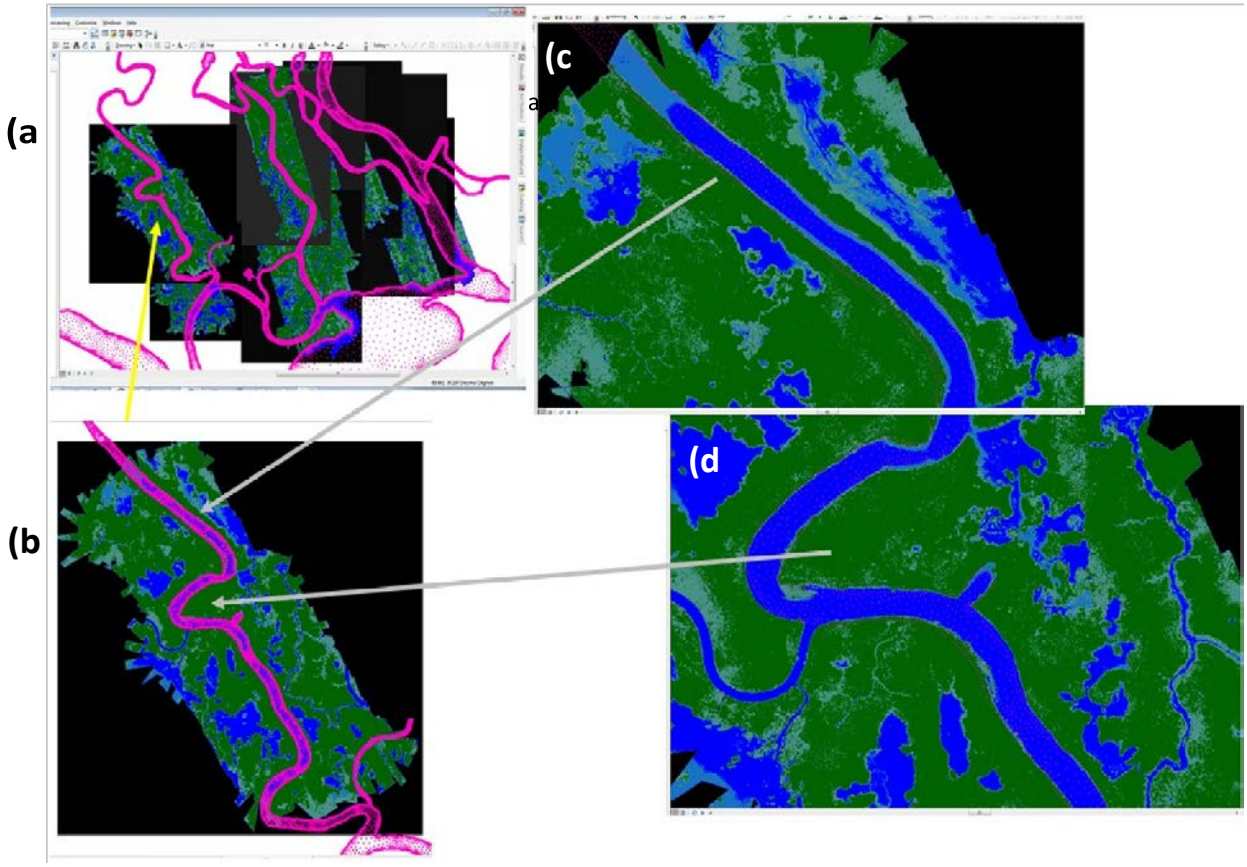

Figure 4 – (a)&(b) West Pearl River channel mesh developed from earlier satellite based remote sensing imagery compared to (c)&(d) a recent (December 2014, Mississippi State University) land/water mask derived from UAS imagery of the West Pearl River and its surrounding floodplain in Louisiana.

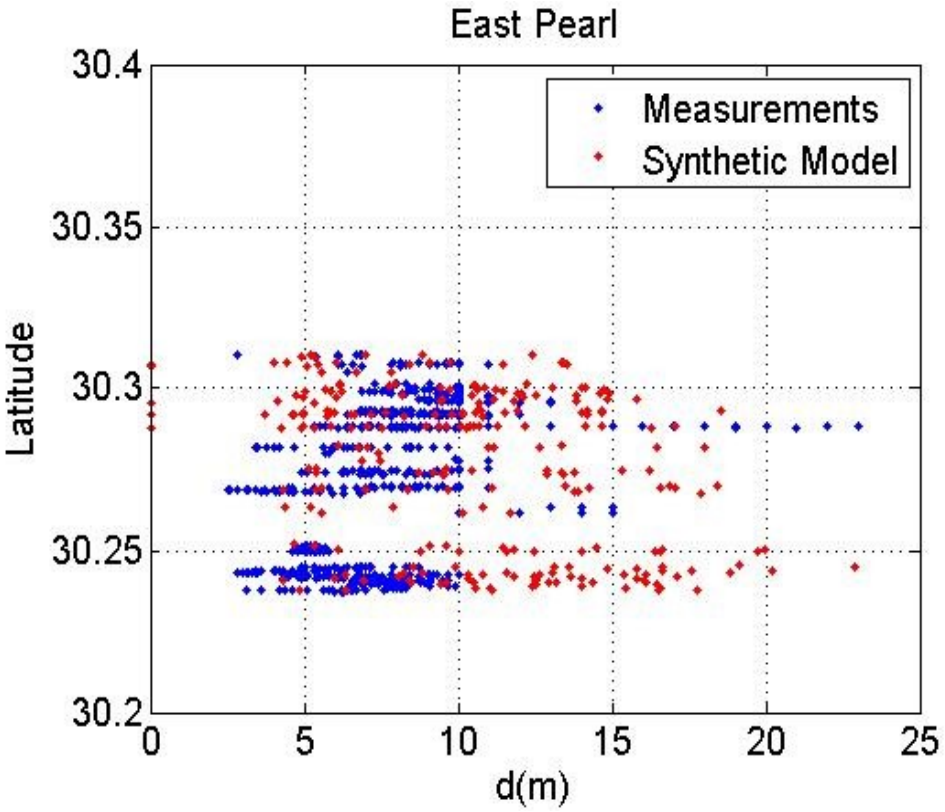

Figure 5 – Synthetic bathymetry (red) compared to measured water depths (blue) on the East Pearl River channel.

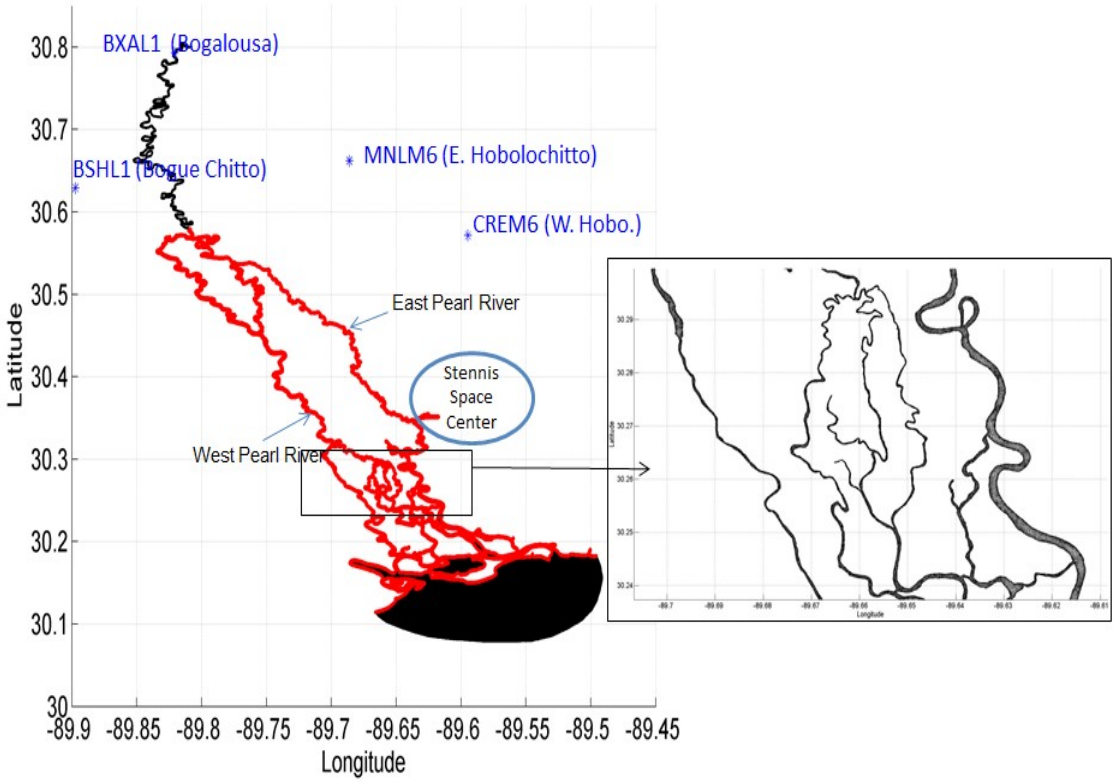

Figure 6 – Pearl River channel mesh (black) with the Bogalusa station (BXAL1) applied as upstream discharge forcing, a truncated version of the channel mesh moving the northernmost boundary just north of the East/West Pearl River split (red), and an inset showing the high resolution mesh detail of the West, Mid-, Middle-, and East (left to right) channels in the Pearl River.

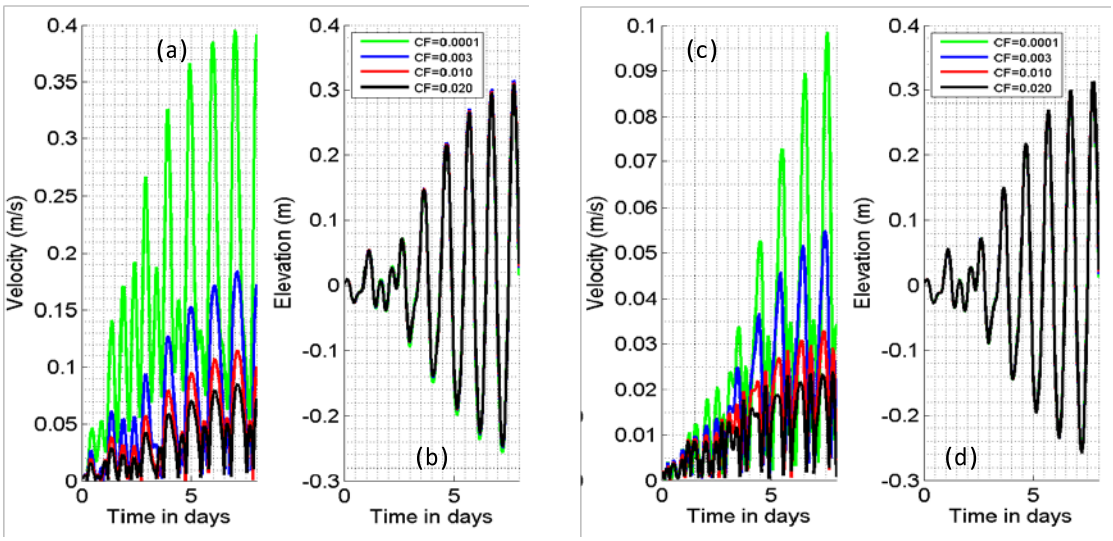

Figure 7 – Modeled currents and water levels using different friction coefficients for (a) Velocity (current) and (b) Elevation (water level) on the West Pearl; (c) Velocity and (d) Elevation on the Middle Pearl.

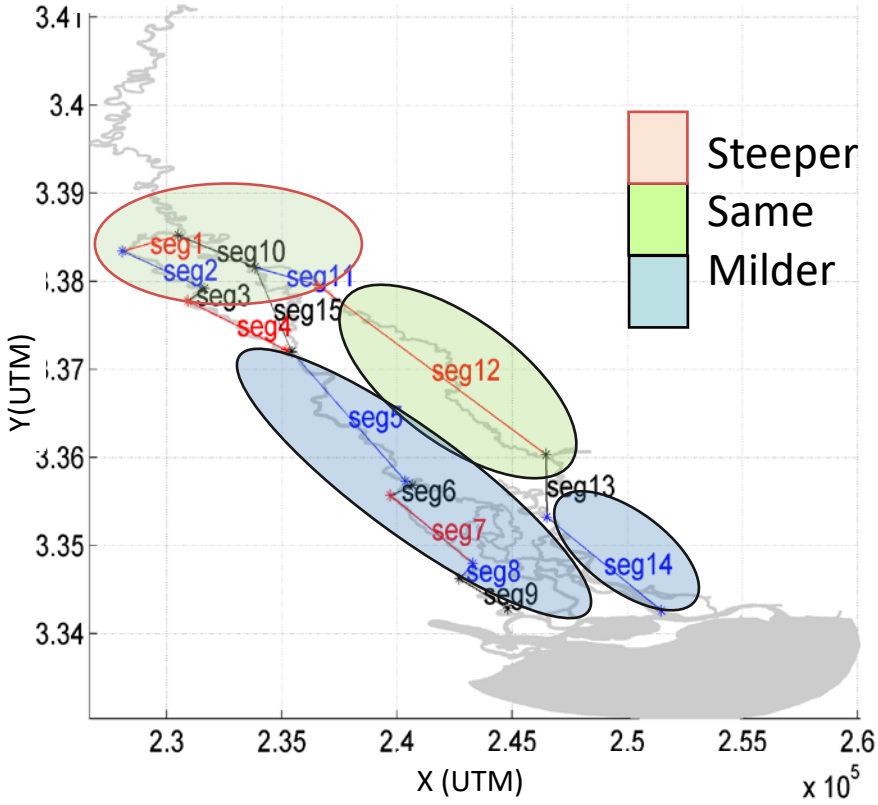

Figure 8 – The variation of topographic slope in the West Pearl and East Pearl river segments compared to the constant representative slope (-3.3832E-04) applied over the entire Pearl River channel model.

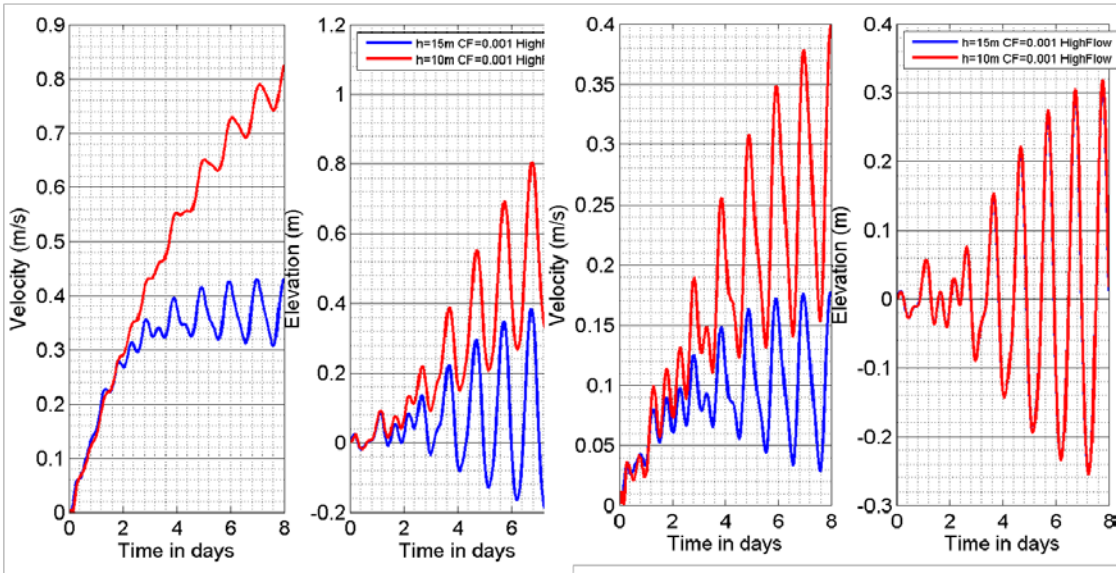

Figure 9 – Modeled currents and water levels using different constant channel water depths (15m vs. 10m) for (a) Velocity and (b) Elevation on the West Pearl; (c) Velocity and (d) Elevation on the East Pearl.

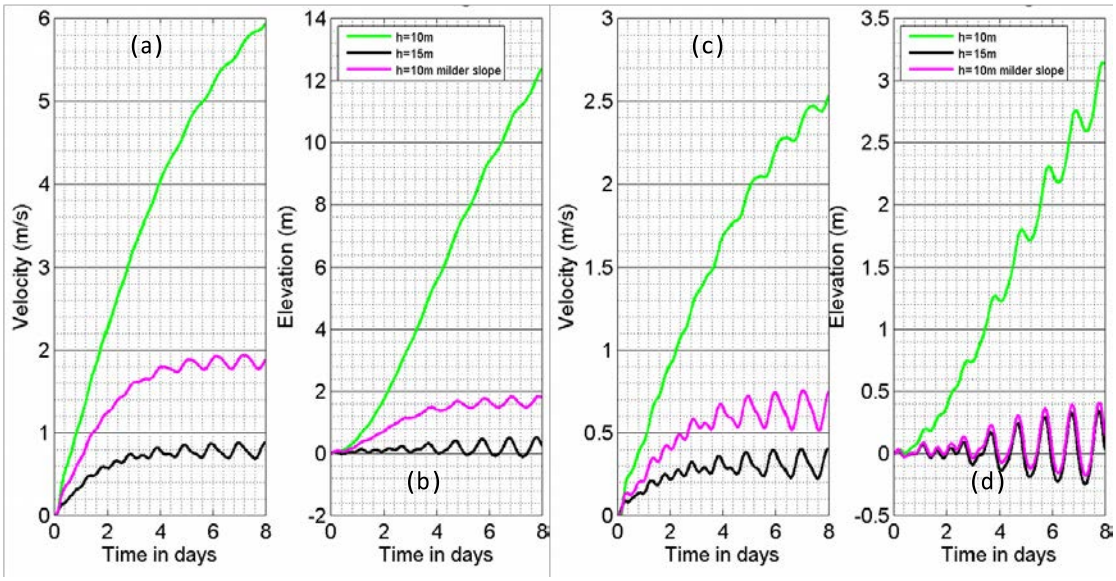

Figure 10 – Modeled currents and water levels using different constant channel water depths (15m vs. 10m) and different slopes (original slope vs. milder slope) for (a) Velocity and (b) Elevation at the W. Pearl; (c) Velocity and (d) Elevation at the E. Pearl.

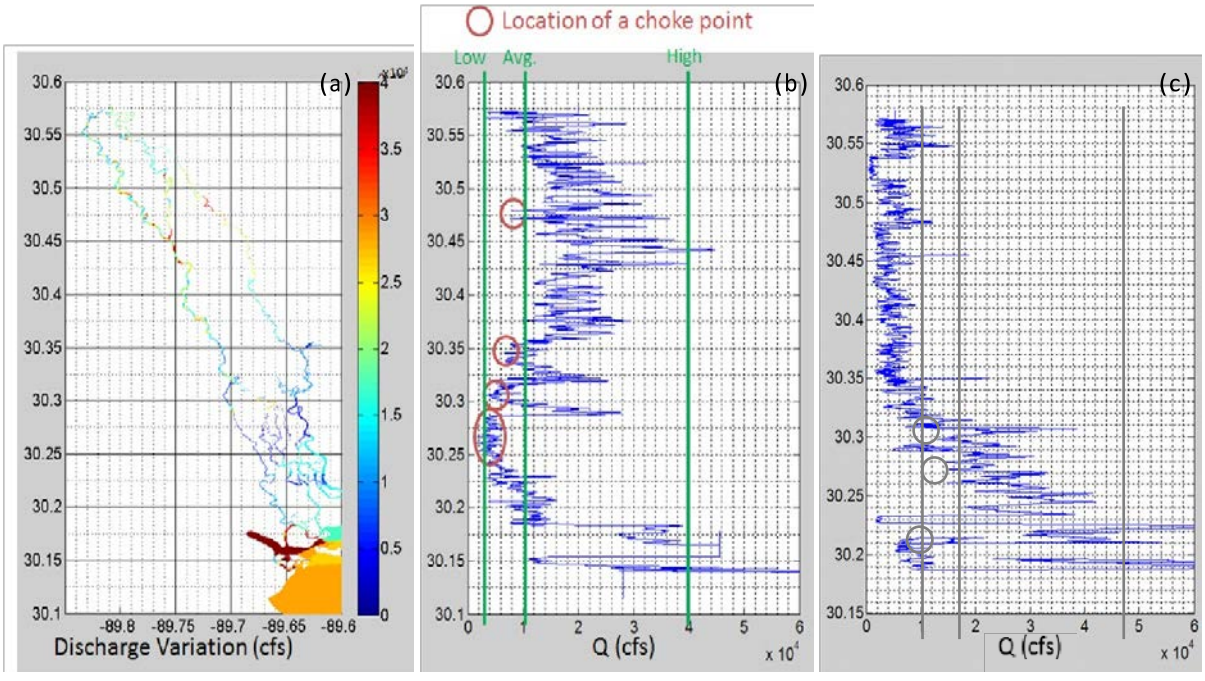

Figure 11 – (a) Discharge capacity variation in the Pearl River channel model (color shading), (b) Discharge capacity of the West Pearl River compared to low, average and high upstream flux conditions (vertical lines), and (c) Discharge capacity of the East Pearl River compared to low, average and high upstream flux conditions (vertical lines).

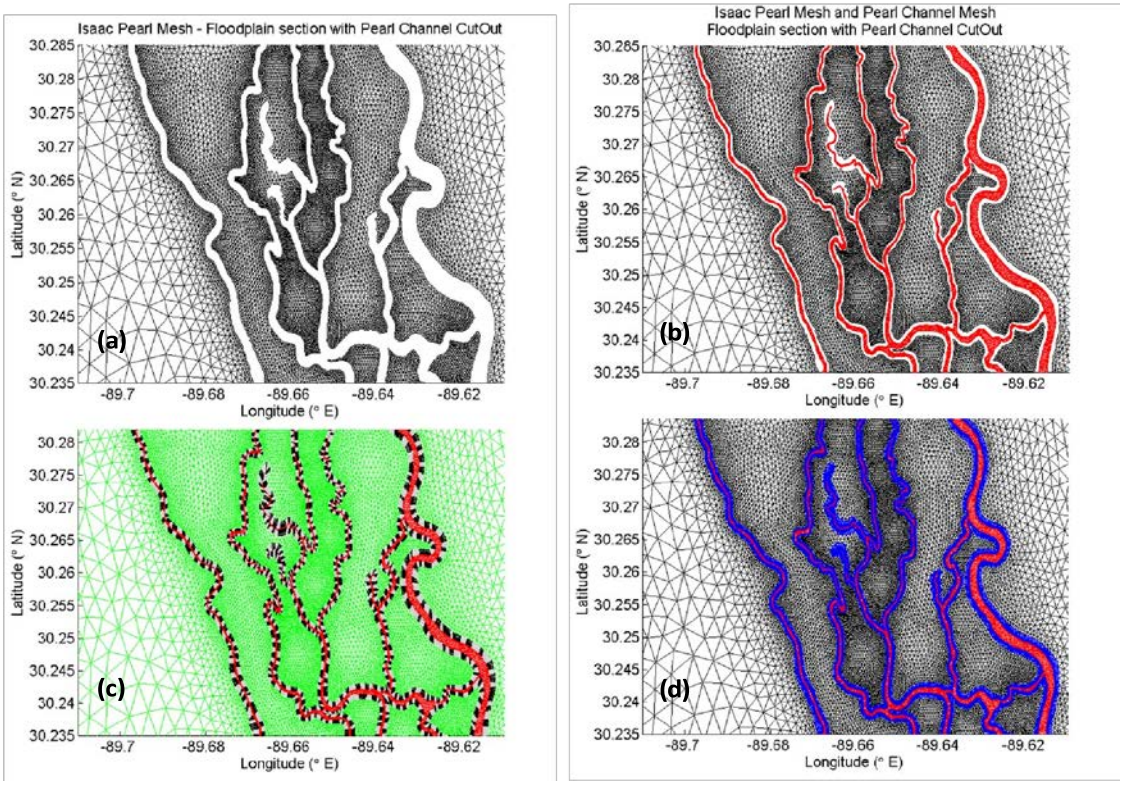

Figure 12 - Stages of mesh development for LPRB floodplain model: (a) Pearl River channel mesh area cut from a larger domain US East Coast mesh (SL16), (b) Pearl River channel mesh inserted into the cut void area, (c) segments (grey and black alternating) used to mesh the transition area between river channel mesh bank nodes and the surrounding US East Coast mesh boundary nodes (d) Pearl River channel mesh with immediate floodplain elements (bold) meshed around the channels and the original floodplain elements of East Coast US mesh.

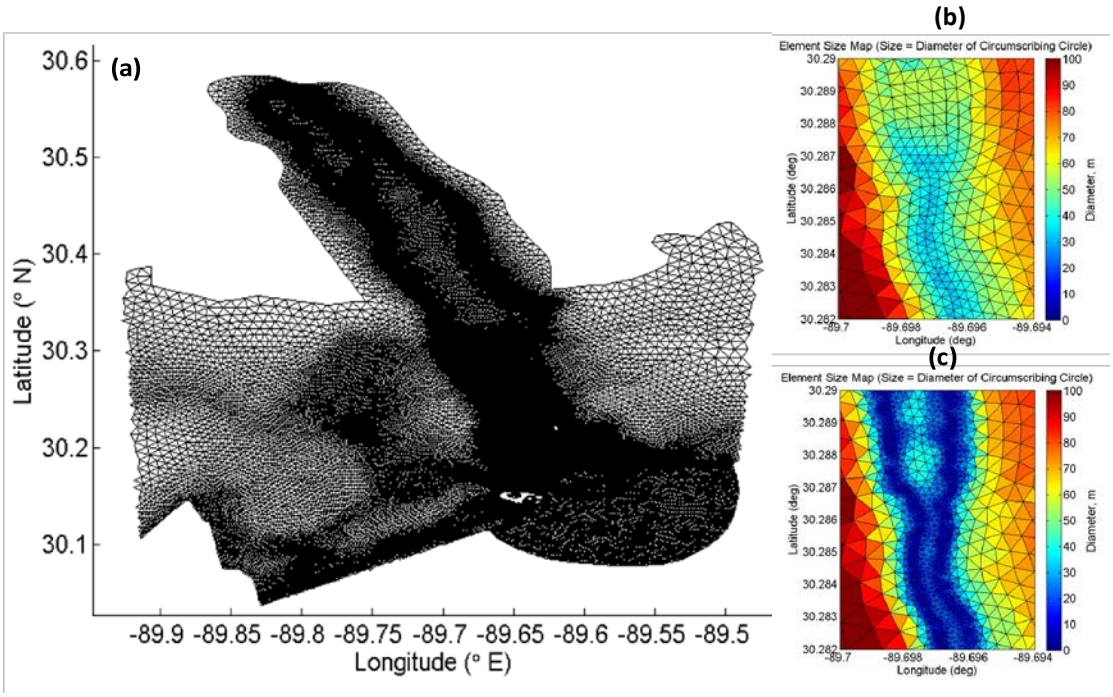

Figure 13 – (a) Mesh of the Lower Pearl River Basin, (b) prior mesh resolution of the larger domain US East Coast model mesh around the Pearl River, (c) new mesh resolution of the floodplain model around the Pearl River.

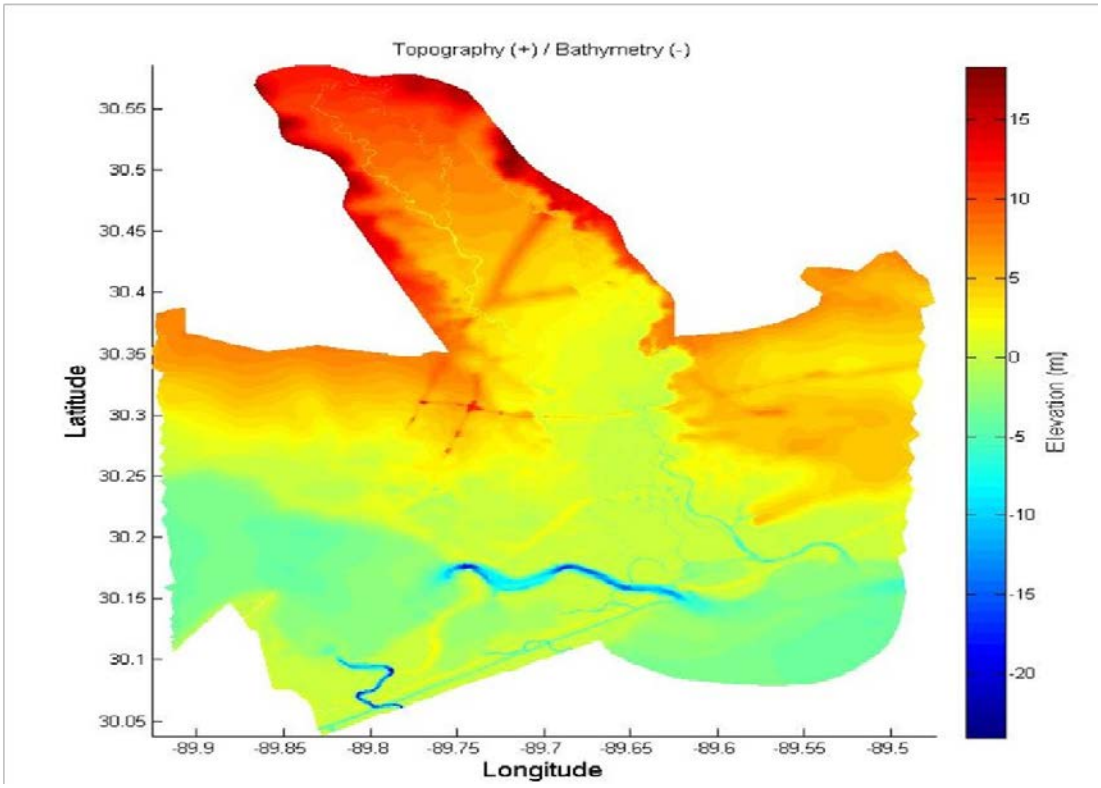

Figure 14 – Bathymetry and topography of the Lower Pearl River Basin floodplain model .

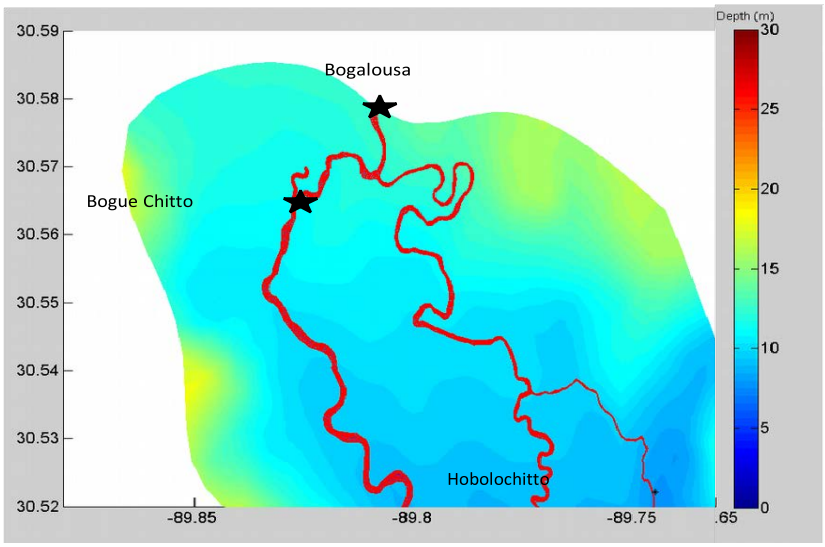

Figure 15 – Upstream bathymetry of the LPRB model near the West and East Pearl River confluence. Active discharge locations (stars), Bogalusa, LA (BXAL1) and Bogue Chitto, LA (BSHL1).

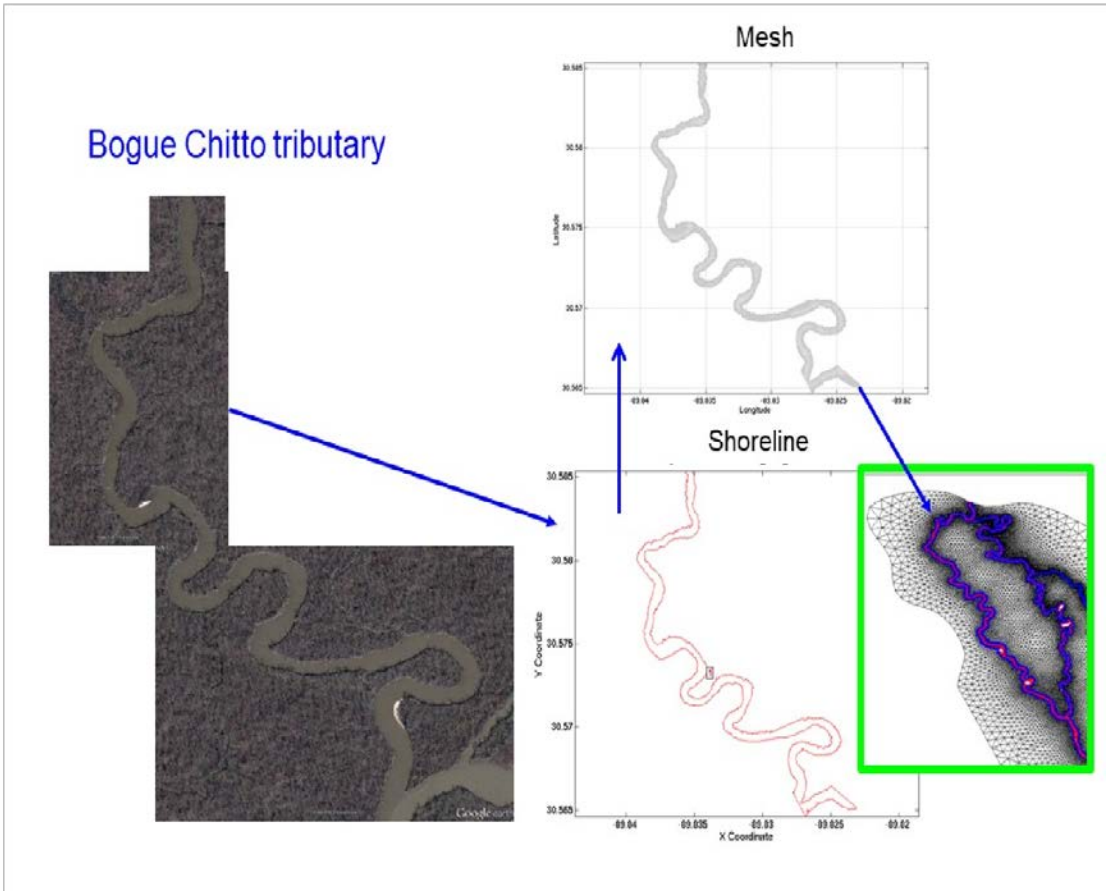

Figure 16 – A demonstration of the imagery analyses techniques of Blain et al. (2013) and Blain and McKay (2014) applied to the Bogue Chitto tributary. The result is that incoming flux from the Bogue Chitto tributary is included in the LPRB model.

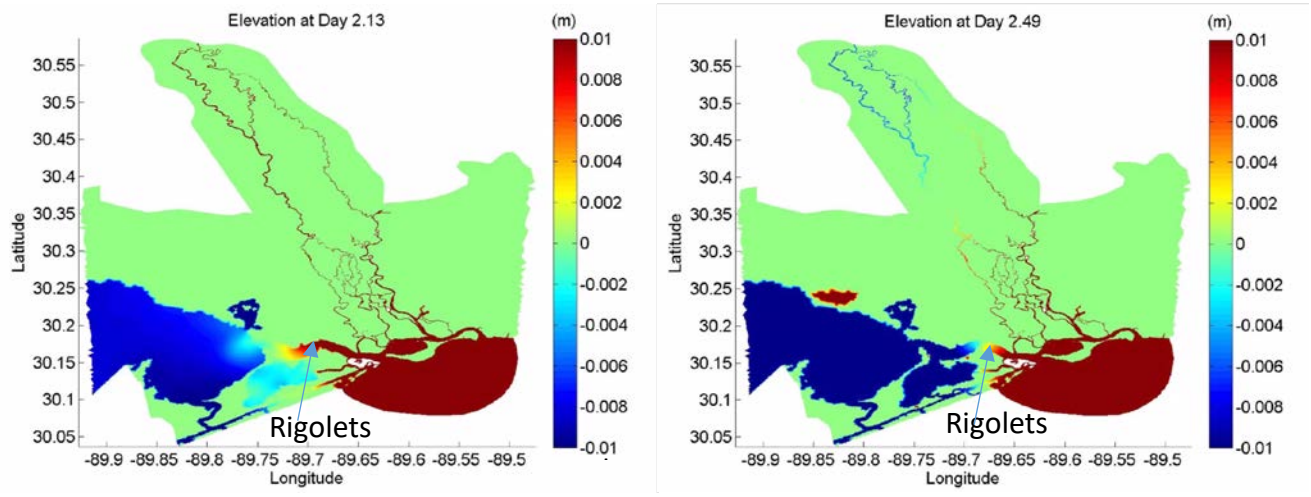

Figure 17 – LPRB model simulation for average flow conditions for (left) 2.2 days and (right) 8 hrs and 40 min. later.

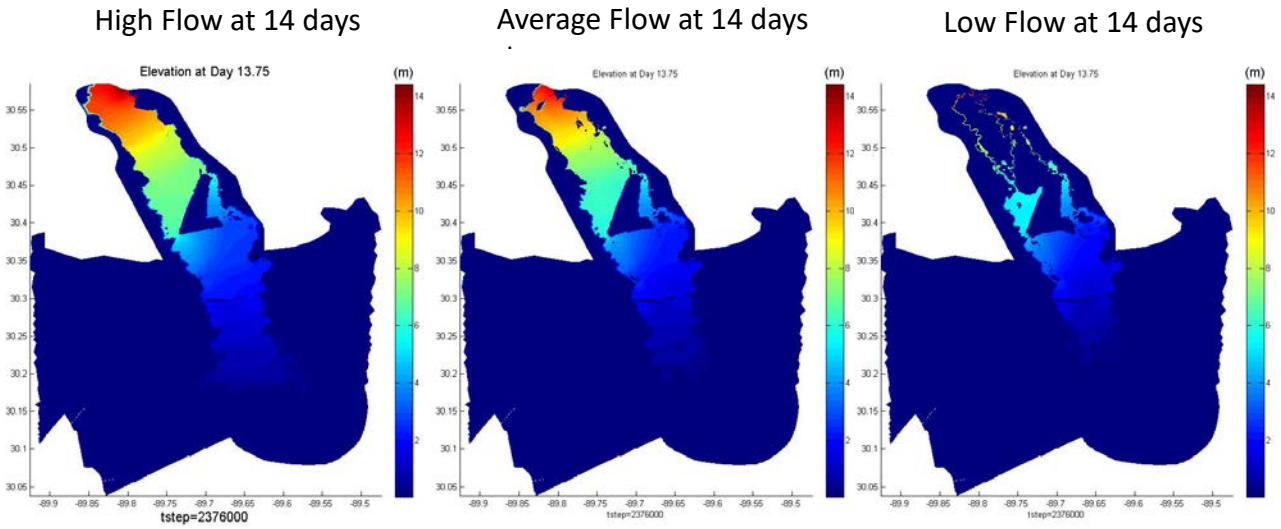

Figure 18 – LPRB model simulation after 14 days for (left) high flow (40,000 cfs), (middle) average flow (10,000 cfs), and, (right) low flow (3000 cfs) conditions.

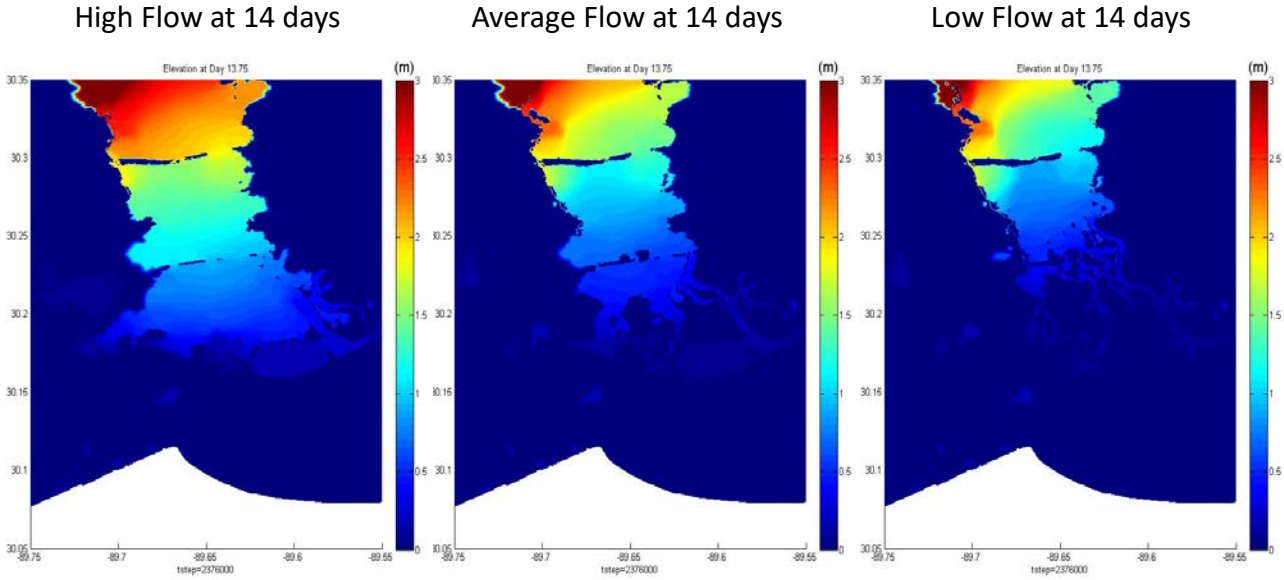

Figure 19 – LPRB model simulation south of Highway 90 after 14 days for (left) high flow (40,000 cfs), (middle) average flow (10,000 cfs), and, (right) low flow (3000 cfs) conditions.

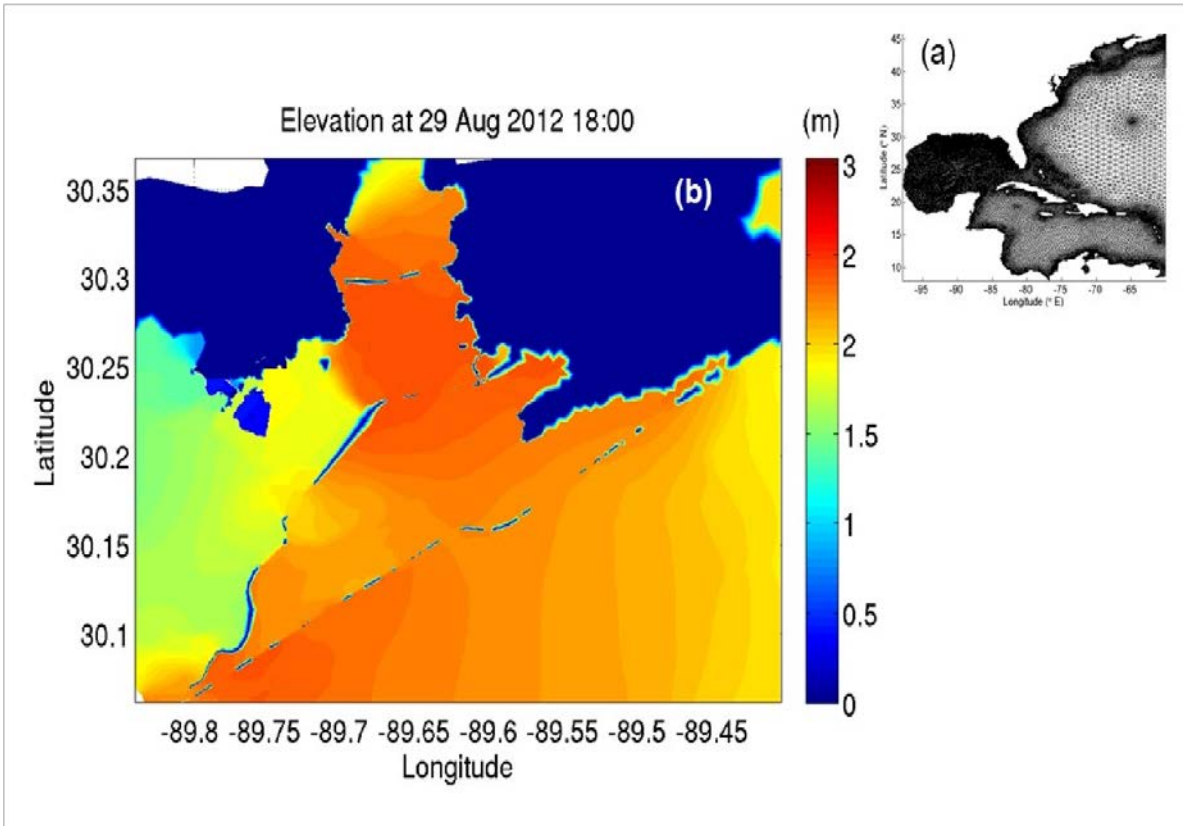

Figure 20 – Louisiana CPRA model simulation of Hurricane Isaac. (a) Large domain CPRA mesh and (b) Maximum water levels over the LPRB just prior to landfall of Hurricane Isaac.

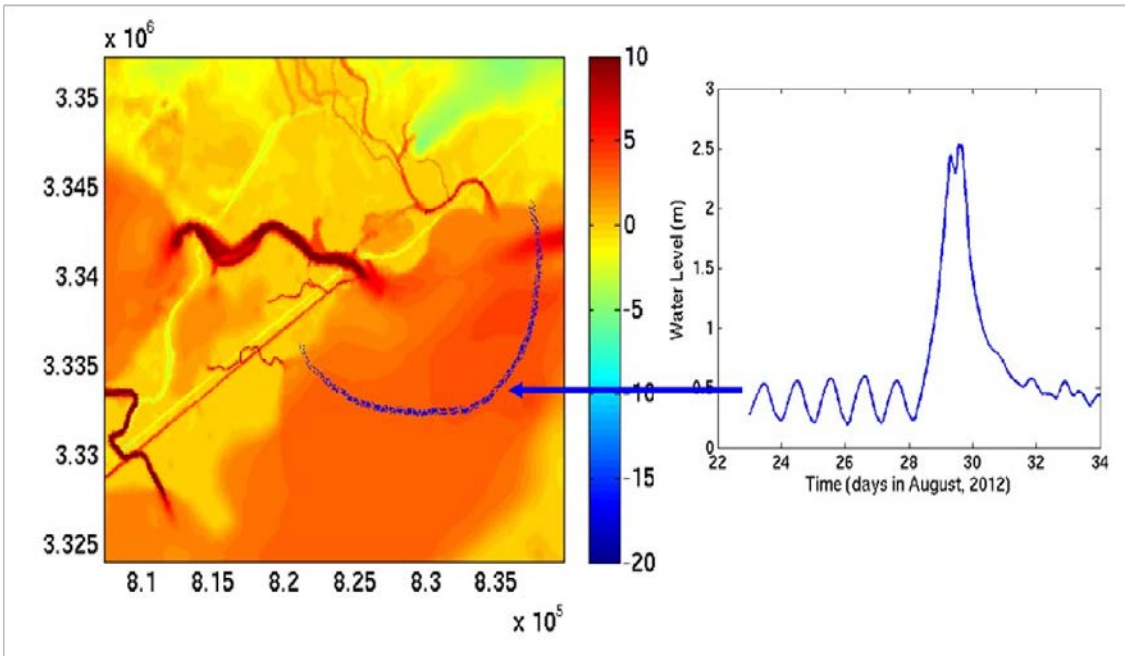

Figure 21 – LPRB open water boundary locations (blue dots) overlain the large domain surge computation (left). An example water level hydrograph (right) for one open water boundary location is shown. All open water boundary points have similar forcing time series extracted from the large domain simulation of Hurricane Isaac.

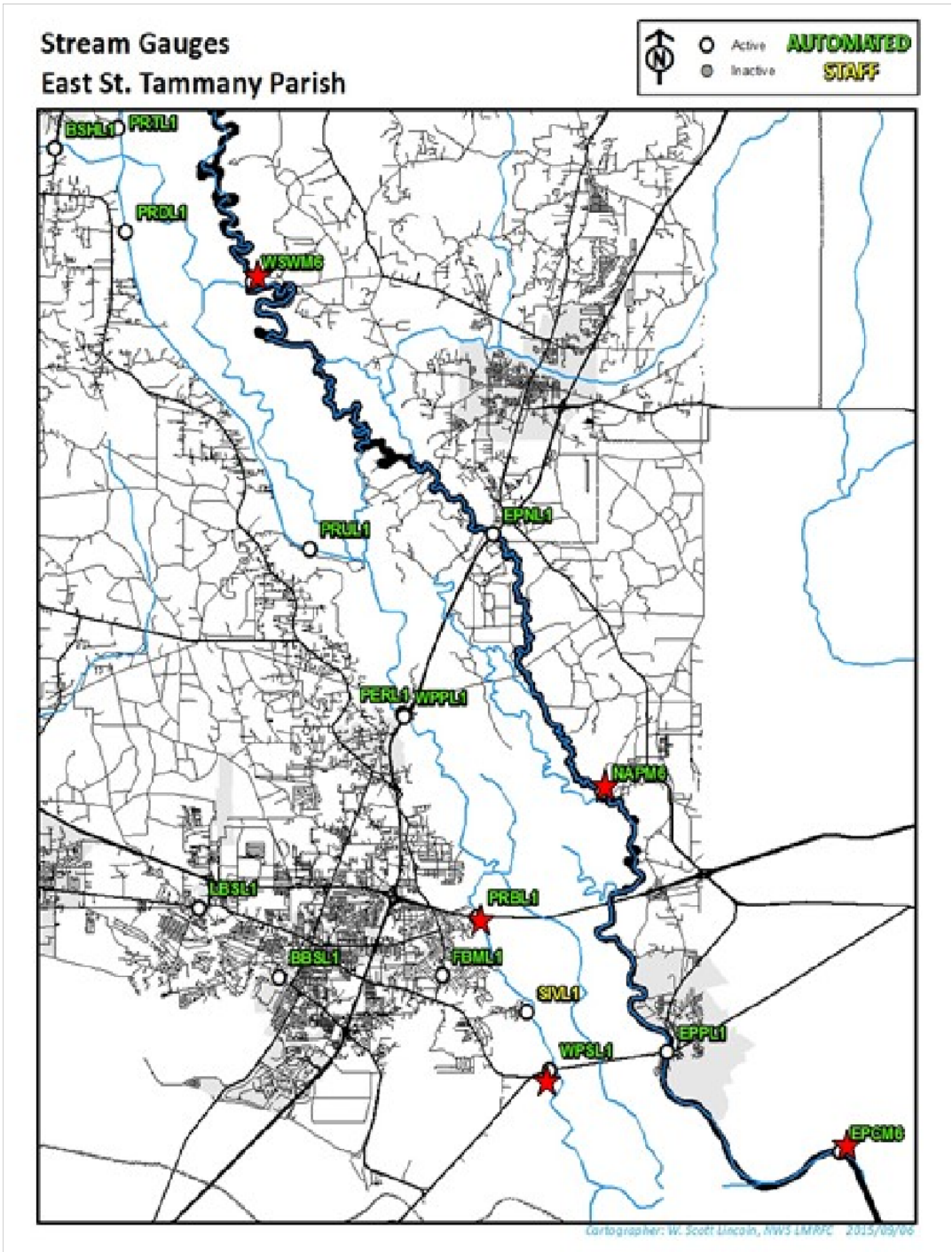

Figure 22 – Five NWS water level gages (stars) active during Hurricane Isaac.

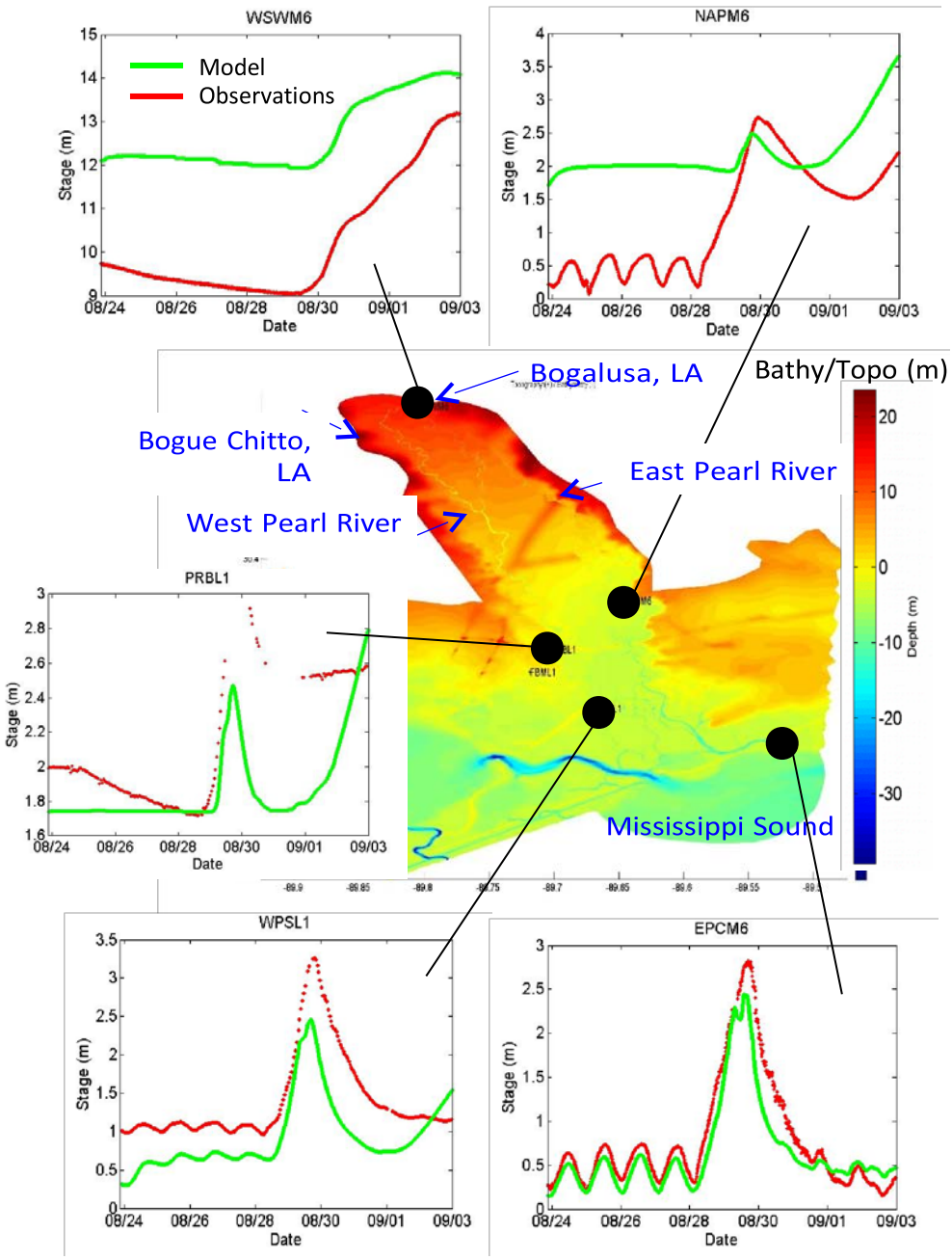

Figure 23 – Water level comparisons during Hurricane Isaac, Aug. 24 – Sep 03, 2012 at 5 NWS hydrograph locations (clockwise from bottom left, WPSL1, PRBL1, WSWM6, NAPM6, and EPCM6). Model computations are green; observations are red. Hydrograph locations (black dots) are shown on LPRB floodplain model bathymetry/topography in meters.

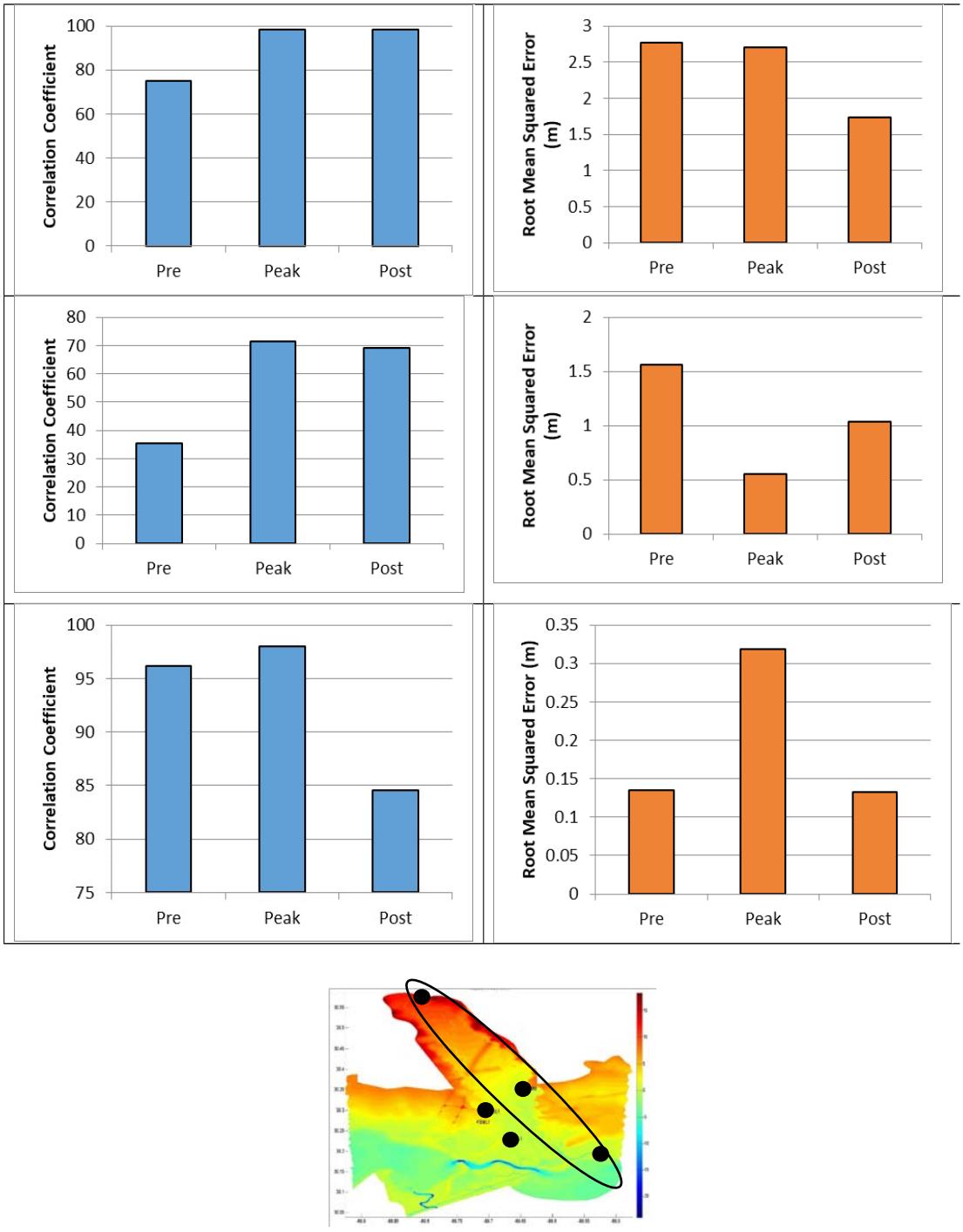

Figure 24 – Water Level Error: Correlation coefficient (blue) and root mean square error (orange) computed during Hurricane Isaac for pre-, peak-, and post- storm time periods at three gages along the West Pearl River north to south (WSWM6, NAPM6, and EPCM6), respectively (circled).

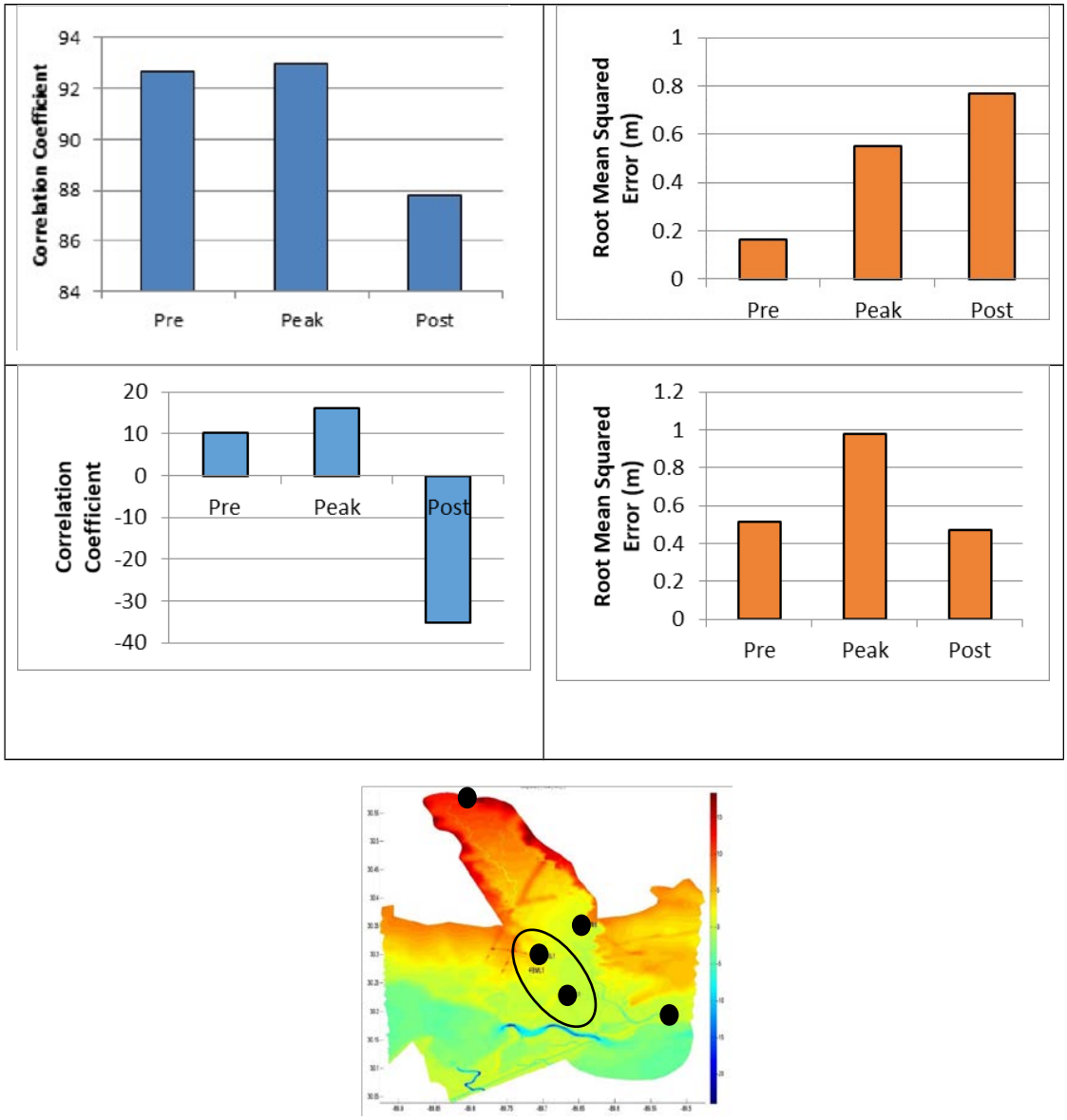

Figure 25 – Water Level Error: Correlation coefficient (blue) and root mean square error (orange) computed during Hurricane Isaac for pre-, peak-, and post- storm time periods at three gages along the West Pearl River north to south (PRBL1 and WPSL1), respectively (circled).

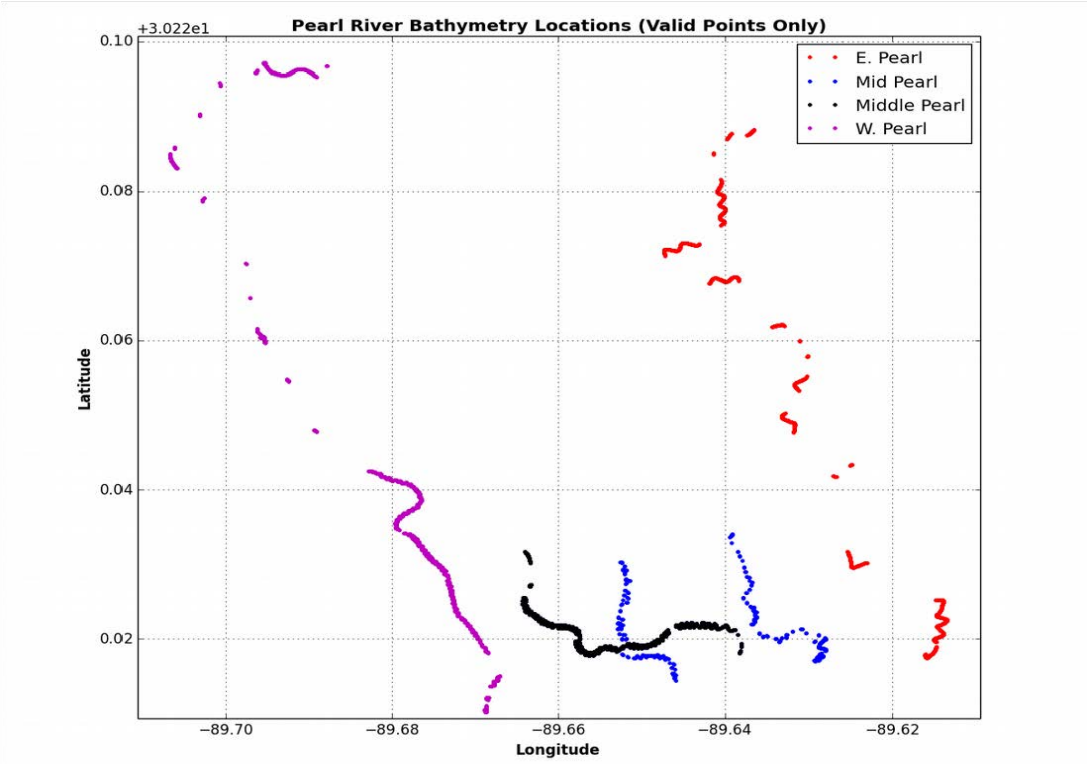

Figure 26 – All locations where water depth measurements were made throughout the LPRB by the St. Tammany Parish Government, LA in 2014 and 2015.